63-2-9

296 874

A. R. A. P.

AERONAUTICAL RESEARCH ASSOCIATES *of* PRINCETON, INC.

ARAP REPORT NO. 47

EXPERIMENTAL INVESTIGATION OF THE STRUCTURE OF VORTICES IN SIMPLE CYLINDRICAL VORTEX CHAMBERS

by

Coleman duP. Donaldson

and

Richard S. Snedeker

This research was supported by the United States Air Force through the Air Force Office of Scientific Research of the Office of Aerospace Research, under Contract Number AF 49(638)-255. Reproduction in whole or in part is permitted for any purpose of the United States Government.

Aeronautical Research Associates of Princeton, Inc.
50 Washington Road, Princeton, New Jersey

December 1962

Abstract

An experimental study of the character of vortices in simple cylindrical vortex chambers completely open at one end is presented. Special attention is given to the problem of the transition from one-celled to two-celled vortex structure. It is shown that for turbulent vortices in vortex chambers having length-to-diameter ratios in the range $0 < L/D < 5$, the character of the flow is primarily dependent on the ratio of a characteristic tangential velocity to a characteristic radial velocity V/U. In addition, it is shown that the Reynolds number based on the radial flow, while a parameter of major importance in laminar vortices, plays but a minor role in turbulent vortex motion. Transition from one-celled to two-celled vortex structure started for all vortex configurations tested ($0 < L/D < 5$) when V/U exceeded approximately 3.

TABLE OF CONTENTS

1. Introduction

Recently, there has been much interest in vortex flows. This interest has been stimulated by the fact that there have been proposed, within the past few years or so, a number of interesting flow devices which depend for their performance on the properties of rapidly rotating, axially symmetric flows. Some of the interesting experimental studies of vortex motions that have been made are those of Kendall (1962), Rosenswieg (1962), Ragsdale (1960), Donaldson (1961), McCune and Williamson (1961), Schowalter and Johnstone (1960), and Keyes (1961).

It is beyond the scope of this paper to attempt a review or critique of all of these recent studies. Suffice it to say that all of them considered in some detail the effects of turbulence on vortex motions and/or the type of axial flow patterns that exist in vortex chambers having specific configurations.

The present paper is no exception. In this paper we shall deal with the motion in simple cylindrical vortex chambers which are completely open at one end. We shall be interested not only in the effects of turbulence on such vortices but also in the behavior and structure of the axial motions that exist.

The present work grew quite naturally out of a rather extensive theoretical study of the characteristics of three-dimensional laminar vortices carried out by the senior author of this paper and his colleagues over the past few years (see Donaldson (1956) and Donaldson and Sullivan (1960)). During the course of these investigations, theoretical solutions were found for both one- and two-celled vortex structures. Since both one- and two-celled vortex structures had been observed in the laboratory and there did not exist in the literature any experimental study specifically aimed at

determining the criteria for transition from one type of flow behavior to the other, the present study was initiated in order to attempt to establish such criteria.

Because of the way in which this study originated, it is felt that it will be helpful if, before describing the experimental apparatus used and the experiments themselves, a very brief review of the basic equations and theoretical results of the previous studies is given.

2. Basic Equations

In this study we will assume that we are dealing with an incompressible fluid of constant viscosity. We will assume axial symmetry so that for a cylindrical coordinate system $(\tilde{r}, \tilde{\phi}, \tilde{z})$ we set the operator $\partial/\partial\tilde{\phi} = 0$. The motion is further assumed to consist of a steady part with velocity components $\tilde{u}$, $\tilde{v}$, and $\tilde{w}$ and a fluctuating part having components $\tilde{u}'$, $\tilde{v}'$, and $\tilde{w}'$ whose time averages are zero. The time averaged equations of motion for the steady part of such a flow satisfy the following set of equations

$$\frac{\partial(\tilde{r}\tilde{u})}{\partial\tilde{r}} + \frac{\partial(\tilde{r}\tilde{w})}{\partial\tilde{z}} = 0 \tag{1}$$

$$\frac{D\tilde{u}}{D\tilde{t}} - \frac{\tilde{v}^2}{\tilde{r}} = -\frac{\partial\tilde{P}}{\partial\tilde{r}} + \nu\left(\tilde{\nabla}^2\tilde{u} - \frac{\tilde{u}}{\tilde{r}^2}\right) - \frac{1}{\tilde{r}}\frac{\partial}{\partial\tilde{r}}(\tilde{r}\overline{\tilde{u}'\tilde{u}'}) - \frac{\partial}{\partial\tilde{z}}(\overline{\tilde{u}'\tilde{w}'}) + \frac{\overline{\tilde{v}'\tilde{v}'}}{\tilde{r}} \tag{2}$$

$$\frac{D\tilde{v}}{D\tilde{t}} + \frac{\tilde{u}\tilde{v}}{\tilde{r}} = \nu\left(\tilde{\nabla}^2\tilde{v} - \frac{\tilde{v}}{\tilde{r}^2}\right) - \frac{1}{\tilde{r}}\frac{\partial}{\partial\tilde{r}}(\tilde{r}\overline{\tilde{u}'\tilde{v}'}) - \frac{\partial}{\partial\tilde{z}}(\overline{\tilde{v}'\tilde{w}'}) - \frac{\overline{\tilde{u}'\tilde{v}'}}{\tilde{r}} \tag{3}$$

$$\frac{D\tilde{w}}{D\tilde{t}} = \frac{\partial\tilde{P}}{\partial\tilde{z}} + \nu\tilde{\nabla}^2\tilde{w} - \frac{1}{\tilde{r}}\frac{\partial}{\partial\tilde{r}}(\tilde{r}\overline{\tilde{u}'\tilde{w}'}) - \frac{\partial}{\partial\tilde{z}}(\overline{\tilde{w}'\tilde{w}'}) \tag{4}$$

Here, $\tilde{P} = \tilde{p}/\rho$, where p is the pressure and ρ is the density, ν is the kinematic viscosity μ/ρ, and the operators $\tilde{\nabla}^2$ and $D/D\tilde{t}$ are

$$\tilde{\nabla}^2 \equiv \frac{\partial^2}{\partial \tilde{r}^2} + \frac{1}{\tilde{r}} \frac{\partial}{\partial \tilde{r}} + \frac{\partial^2}{\partial \tilde{z}^2}$$

$$\frac{D}{D\tilde{t}} \equiv \frac{\partial}{\partial \tilde{t}} + \tilde{u}\frac{\partial}{\partial \tilde{r}} + \tilde{w}\frac{\partial}{\partial \tilde{z}}$$

The correlations of the form $\overline{\tilde{u}'\tilde{u}'}$, $\overline{\tilde{u}'\tilde{v}'}$, etc. are the negatives of the usual Reynolds stress terms divided by the density (see Lamb (1932) pp. 674-678).

Some very general conclusions concerning this set of equations can be drawn from an examination of their non-dimensional form. In order to put equations (1) through (4) in this form, it is necessary to make some assumptions concerning the proper parameters by which the Reynolds stress terms are to be made non-dimensional. We first note, however, that in view of equation (1), u and w are closely connected so that the magnitude of u orders the magnitude of w. We thus choose a reference radial velocity U and define

$$\begin{aligned} \tilde{u} &= Uu(r, z) \\ \tilde{w} &= Uw(r, z) \end{aligned} \tag{5}$$

where $r = \tilde{r}/R$ and $z = \tilde{z}/R$ are non-dimensional coordinates defined in terms of the reference length R. Since the magnitude of the tangential velocity v is not ordered by either u or w, we choose a second reference velocity V

for the tangential motion and set

$$\tilde{v} = Vv(r, z) \tag{6}$$

We may now return to the question of the non-dimensionalization of the Reynolds stress terms. We will assume that these stresses are functions of the related rates of deformation. When account is taken of the axial symmetry, these deformation rates and the reference velocity on which they depend are

$$\begin{aligned}
\epsilon_{rr} &= \frac{\partial \tilde{u}}{\partial \tilde{r}} \sim U \\
\epsilon_{\phi\phi} &= \frac{\tilde{u}}{\tilde{r}} \sim U \\
\epsilon_{zz} &= \frac{\partial \tilde{w}}{\partial \tilde{z}} \sim U \\
\epsilon_{r\phi} &= \frac{1}{2}\left(\frac{\partial \tilde{v}}{\partial \tilde{r}} - \frac{\tilde{v}}{\tilde{r}}\right) \sim V \\
\epsilon_{\phi z} &= \frac{1}{2}\left(\frac{\partial \tilde{v}}{\partial \tilde{z}}\right) \sim V \\
\epsilon_{rz} &= \frac{1}{2}\left(\frac{\partial \tilde{u}}{\partial \tilde{z}} + \frac{\partial \tilde{w}}{\partial \tilde{r}}\right) \sim U
\end{aligned} \tag{7}$$

In view of the relationships exhibited in equations (7), we will make the Reynolds stress terms non-dimensional according to the following scheme

$$\begin{aligned}
\overline{-u'u'} &= U^2\sigma_{11}(r, z) \\
\overline{-v'v'} &= U^2\sigma_{22}(r, z) \\
\overline{-w'w'} &= U^2\sigma_{33}(r, z) \\
\overline{-u'v'} &= V^2\sigma_{12}(r, z) \\
\overline{-v'w'} &= V^2\sigma_{23}(r, z) \\
\overline{-u'w'} &= U^2\sigma_{13}(r, z)
\end{aligned} \tag{8}$$

In order to make the pressure dimensionless, we note that, according to equation (2), a part of the static pressure must balance the centrifugal forces which are proportional to the square of the tangential velocity. On the other hand, according to equation (4), a part of the pressure must account for the acceleration of the fluid in the axial direction. We will thus write

$$\tilde{P} = V^2 P_1(r, z) + U^2 P_2(r, z) \tag{9}$$

In terms of the non-dimensional quantities defined above, the basic equations (1) through (4) become (with $t = \tilde{t}U/R$)

$$\frac{\partial(ru)}{\partial r} + \frac{\partial(rw)}{\partial z} = 0 \tag{10}$$

$$\left(\frac{U}{V}\right)^2 \frac{Du}{Dt} - \frac{v^2}{r} = -\frac{\partial P_1}{\partial r} - \left(\frac{U}{V}\right)^2 \frac{\partial P_2}{\partial r} + \frac{\nu}{UR}\left(\frac{U}{V}\right)^2 \left(\nabla^2 u - \frac{u}{r^2}\right) + \left(\frac{U}{V}\right)^2 \left(-\frac{\sigma_{22}}{r} + \frac{1}{r}\frac{\partial}{\partial r}(r\sigma_{11}) + \frac{\partial \sigma_{13}}{\partial z}\right) \tag{11}$$

$$\frac{Dv}{Dt} + \frac{uv}{r} = \frac{\nu}{UR}\left(\nabla^2 v - \frac{v}{r^2}\right) + \left(\frac{V}{U}\right)\left(\frac{1}{r^2}\frac{\partial}{\partial r}(r^2\sigma_{12}) + \frac{\partial \sigma_{23}}{\partial z}\right) \tag{12}$$

$$\frac{Dw}{Dt} = -\left(\frac{V}{U}\right)^2 \frac{\partial P_1}{\partial z} - \frac{\partial P_2}{\partial z} + \frac{\nu}{UR}\nabla^2 w + \frac{1}{r}\frac{\partial}{\partial r}(r\sigma_{13}) + \frac{\partial \sigma_{33}}{\partial z} \tag{13}$$

We may make the following observations from the system of equations (10) through (13). Firstly, the fluid motions are given completely in terms of just two parameters. These parameters are a Reynolds number $N = UR/\nu$ based on the reference radial velocity and a characteristic radial dimension, and the ratio U/V, i.e. the ratio between the characteristic radial and tangential velocities. Secondly,

for high Reynolds numbers when the Reynolds stresses are dominant, we would expect the parameter U/V to become the controlling factor in determining the motion. This statement must be qualified somewhat. We can never expect the ratio U/V to become the sole parameter governing the motion at high Reynolds numbers since the stress functions σ_{ij} must themselves be weakly dependent on Reynolds number. In addition, the viscous term $(\nu/UR)\nabla^2 w$ in equation (13) will turn out, in the particular flows we will investigate here, to behave in a boundary-layer-like manner and hence the Reynolds number N remains an important parameter although, as we shall see, it is not the primary parameter in governing the motions.

We may also make the following general observation concerning the tangential velocities which are governed by equation (12). We note from this equation that if both the laminar and turbulent stresses are absent ($\nu = 0$ and $\sigma_{ij} = 0$), then the product vr remains constant along all streamlines. Thus, if the radial flow is inward, we would obtain a truly vortex-like behavior. That is, the tangential velocity would increase inversely with radius as the flow proceeded towards the axis of symmetry. If only laminar stresses are present ($\nu \neq 0$ and $\sigma_{ij} = 0$), the tangential velocity must vanish at $r = 0$ but the flow will become more vortex-like the higher the Reynolds number $\rho UR/\mu$. Since the mass flow into a vortex per unit length in the z direction is proportional to ρUR, we would expect to obtain more vortex-like behavior of such flows the higher we made the inward radial mass flow regardless of what the tangential velocity is. Experimentally, this type of behavior is not, in general, observed. The reason is that, for the usual vortex experiments, the Reynolds number is sufficiently high so that the vortex is turbulent and the

stresses which dominate the viscous behavior are the Reynolds stresses. Turning our attention to equation (12) for the case of large Reynolds number, we see that the parameter governing the viscous behavior of the vortex is U/V. In other words, for turbulent vortices to have a more vortex-like behavior, i.e. tangential velocities approaching a $1/r$ dependence, we would want to make the ratio U/V large, and we would expect flows in which U/V was small to behave in a manner somewhat similar to a very viscous laminar vortex. We will see in what follows that this rather general observation obtained from dimensional considerations is supported by experimental results.

3. Boundary Conditions and Existing Solutions

In the present experimental study, we are interested in the behavior of the steady flow in a cylindrical vortex chamber which is let into an otherwise plane surface (see figure 1). Let the depth of this vortex chamber be L and its inside radius R. The tangential motion is introduced by rotation of the porous cylinder through which a radial flow is maintained by virtue of a pressure differential across the porous wall. Let the tangential velocity at R be V, where V is independent of $\tilde{z}$. It is possible to arrange matters experimentally so that the radial velocity at $\tilde{r} = R$ is approximately independent of $\tilde{z}$. Let this radial velocity at R have magnitude U.

At the present time, it is hopeless to seek a solution of equations (10) through (13) that is valid for both the region inside and outside (above) the vortex cup just described. The best that can be done is to seek solutions to related problems having far simpler boundary conditions and to use these solutions to draw inferences concerning the behavior of the more general problem.

Since, experimentally, one finds that what happens in the region exterior to the vortex cup depends on the type of flow produced within the vortex cup, it would seem logical to seek solutions that would be approximately valid within the vortex chamber. Even this simplified problem is, in general, very difficult because of the behavior of the viscous boundary layers on the floor of the vortex cup. If these effects are neglected we obtain a problem which, at least for the case of laminar flow, is tractable from the point of view of analysis.

Following this line of reasoning, if we neglect the end effects of both the open and closed ends of the vortex chamber, we should seek a steady solution to equations (10)

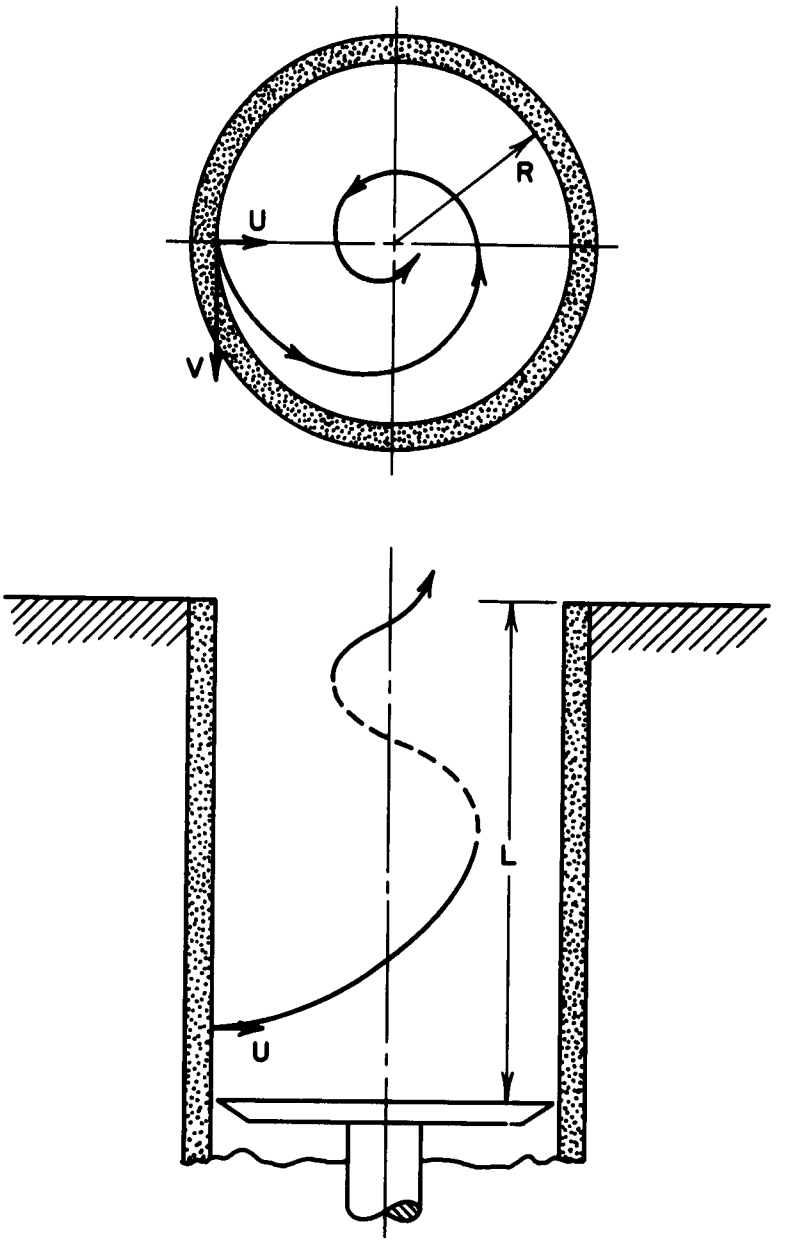

Figure 1. Vortex chamber geometry.

through (13) subject to the following boundary conditions

$$\begin{aligned} u(1, z) &= 1 \qquad & u(0) &= 0 \\ v(1, z) &= 1 \qquad & v(0) &= 0 \\ w(1, z) &= 0 \qquad & & \\ w(r, 0) &= 0 \qquad & \left(\frac{\partial w}{\partial r}\right)_{r=0} &= 0 \end{aligned} \tag{14}$$

For the case of laminar flow ($\nu \neq 0$, $\sigma_{ij} = 0$), such motions have been studied extensively by Donaldson (1956) and by Donaldson and Sullivan (1960). The motions are such that the radial and tangential velocities are independent of z while the axial velocity is of the form $w = zf(r)$. The pressures P_1 and P_2 are of the form

$$\begin{aligned} P_1 &= P_1(r) \\ P_2 &= Cz^2 \end{aligned} \tag{15}$$

where C is a constant. Under these conditions, equations (10) and (13) become independent of (11) and (12); that is, the radial and axial motions become independent of the tangential motion. Once equations (10) and (13) are solved for $u(r)$ and $f(r)$, equation (12) may be solved for the tangential motion, $v = v(r)$. Finally, equation (11), from which the term containing P_2 disappears, may be solved for the pressure P_1 which is associated with the balancing of certrifugal forces, radial accelerations, and stresses acting in the radial direction.

The most interesting single feature of the results of Donaldson and Sullivan's study which is of importance here is the fact that they found that for inward directed radial flows there existed two distinct solutions for the motion in the vortex chamber corresponding to either a one- or

two-celled flow configuration as illustrated in figure 2. There is nothing in the solutions themselves to indicate which of these two motions is preferred. However, given a vortex chamber of finite length L such as is shown in figure 1, one can reason what might determine the transition from one- to two-celled flow.

Consider the vortex chamber and the flow emanating from it shown in figure 3. For zero or very small tangential velocities of the chamber wall, the streamlines are very much as shown. The flow leaves the vortex chamber almost parallel to the axis of symmetry and, as it does so, it entrains by viscous action a certain amount of the gas in the region into which it flows. The pressure just outside the exit of the vortex chamber at point A will be equal to ambient pressure far from the vortex chamber. At the point B on the centerline in the exit plane, the static pressure will differ from that at A by an amount which can be found by integrating equation (11) with respect to r from the centerline to the full radius R. For zero rotation the static pressure at B is slightly higher than the pressure at A due to the decelleration of the radial flow. As the chamber wall is rotated faster and faster, the pressure at B drops rapidly due to the necessity of balancing the centrifugal forces. Obviously, for a given V, this pressure drop will be larger the more vortex-like the tangential velocity profile becomes. Now let us consider the total pressure at B. The total pressure at B will be made up of the static pressure at B plus the dynamic pressure due to the axial component of velocity along the centerline. Since this axial flow at the exit plane of the vortex chamber must account for all the flow that entered through the sides of the chamber, the average velocity in the exit plane $\overline{w}$ must be given by

$$\pi R^2 \overline{w} = 2\pi RLU$$

or

$$\overline{w} = 2\pi \frac{L}{R} U$$

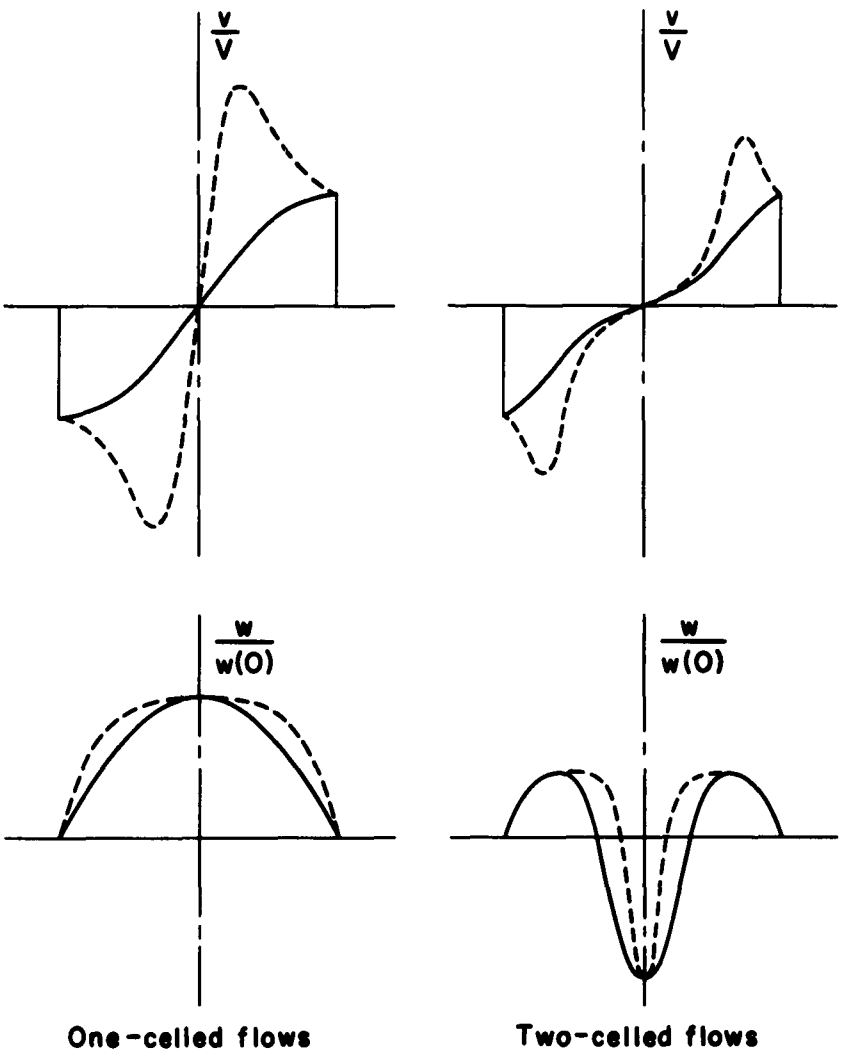

Figure 2. Typical tangential and axial velocities in one- and two-celled vortices after Donaldson and Sullivan (1960).

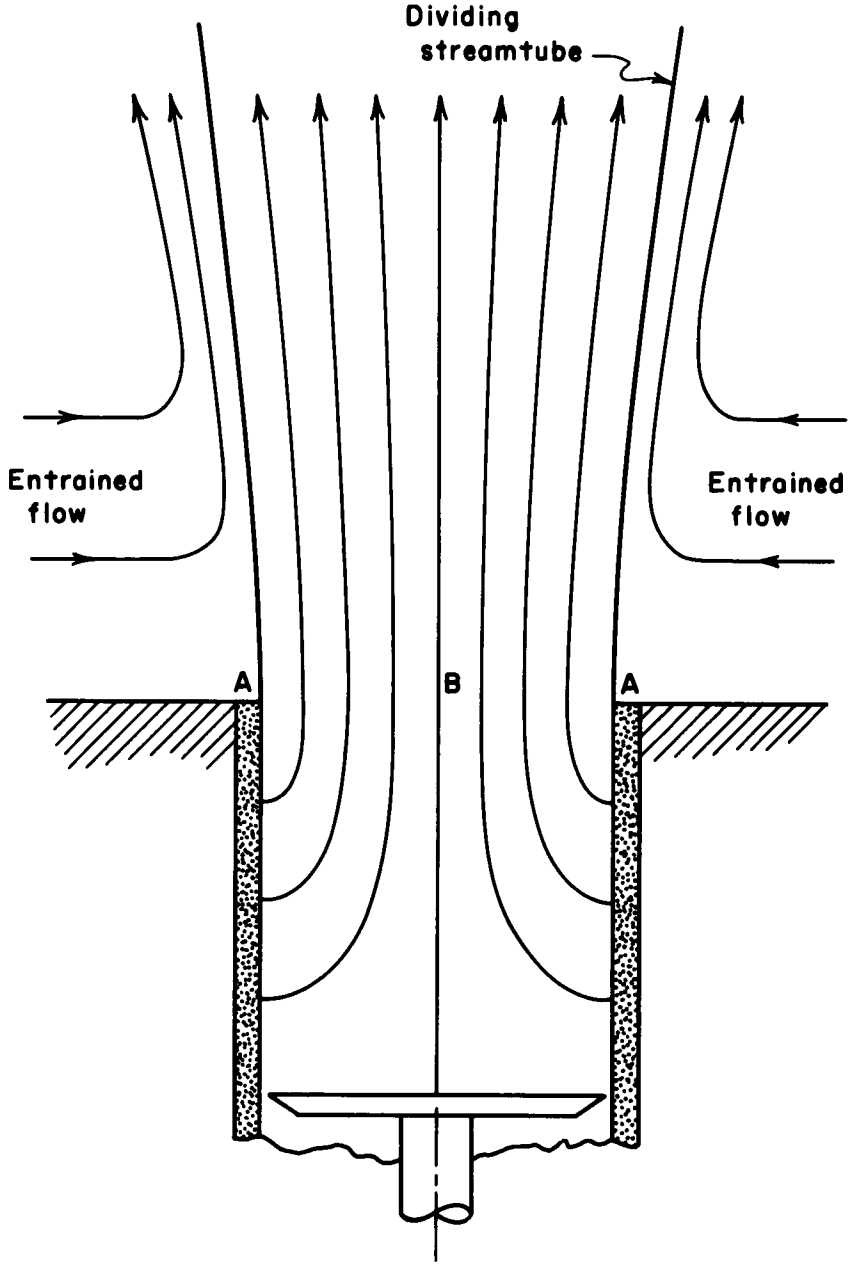

Figure 3. Schematic view of streamline pattern for nonrotating vortex chamber.

Thus for a given radial flow U we would expect the dynamic pressure at the point B to be proportional to the square of the length-to-diameter ratio (L/D) of the vortex chamber.

Now for a given chamber, let us follow what happens to the total pressure at the point B as the vortex chamber is taken from zero to a high rotational velocity. Initially, with V = 0, the total pressure is higher than ambient pressure by an increment that is made up of two parts; a static part arising from the terms containing u in equation (10) and a dynamic part arising from the mass flow leaving the chamber. When the vortex chamber is rotated, the static pressure at B drops. It may in fact, for a given depth of chamber, drop so much that the total pressure at B is less than the ambient pressure into which the vortex chamber is exhausting. In such a case, the one-celled flow we have been envisioning cannot exist. We must suppose instead that a two-celled flow exists. Actually, due to the finite length of a real vortex chamber and the attendant end effects, this transition from one- to two-celled flow does not occur suddenly. As we shall see from the experimental results presented later, as the velocity of rotation is increased, a second cell starts well above the vortex chamber and is gradually sucked into the center of the vortex chamber itself.

These ideas may perhaps be somewhat clearer if we present a few numerical results based on the theoretical solutions of Donaldson and Sullivan. In figure 4 there is plotted as a function of V/U the non-dimensional pressure difference between the static pressures at the exit plane and on the centerline (point B) of a vortex chamber having a length-to-diameter ratio of five. As mentioned before, two parameters (V/U and N) govern the motion so that the

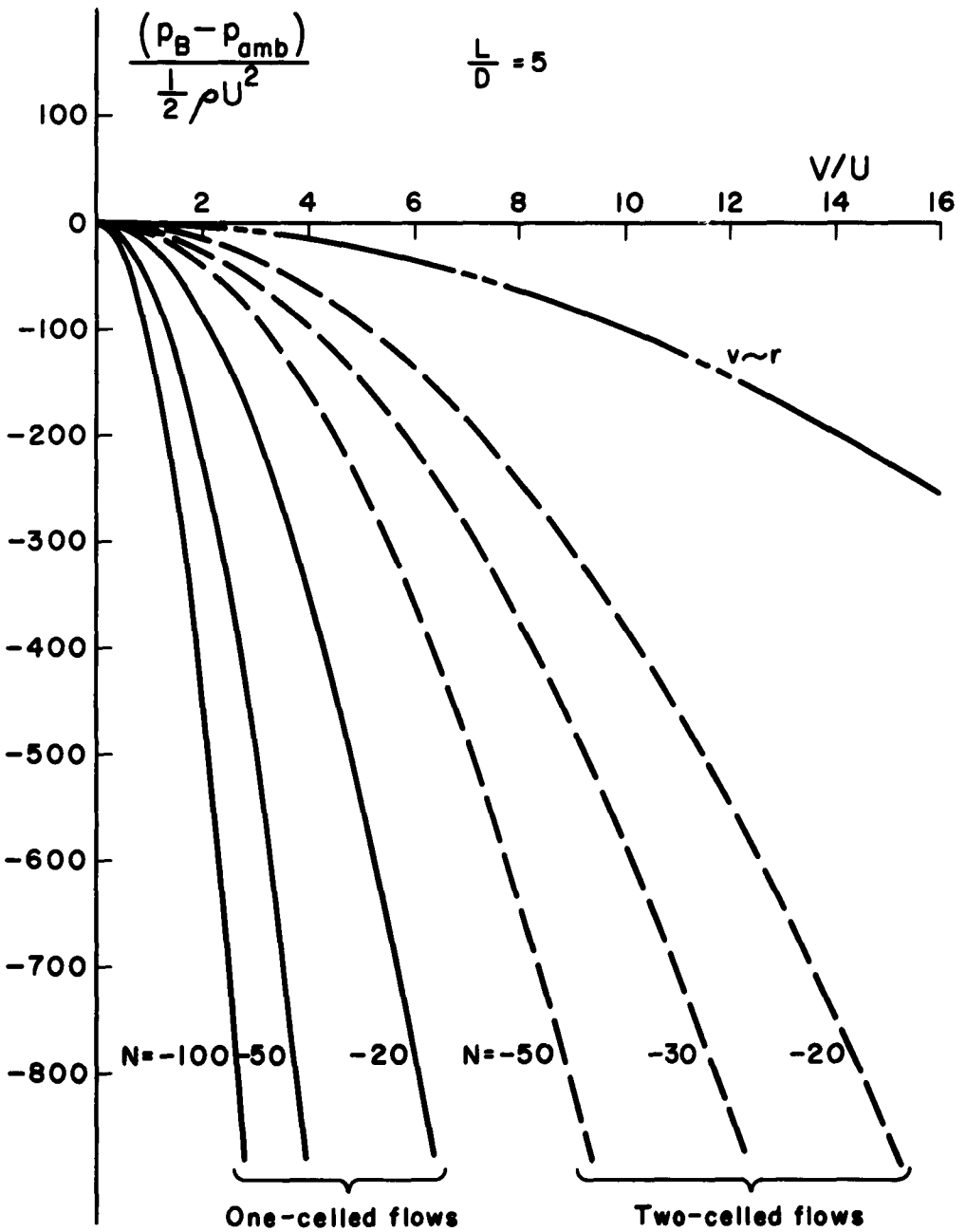

Figure 4. Static pressure at the center of the exit plane (point B) as a function of V/U based on the solutions of Donaldson and Sullivan.

Reynolds number N appears as an independent parameter. As expected the static pressure drops off as the square of V/U in order to balance the centrifugal forces. Also as expected for each family of vortices the pressure drop is more rapid the higher the numerical value of the Reynolds number (the Reynolds number N is negative by convention since inward velocities carry a negative sign). Also included on figure 4 for comparison is the curve showing the static pressure drop that would be experienced if the vortex were not to turn in a vortex-like manner at all, but were to have infinite viscosity and hence turn within the vortex chamber as a solid body.

The critical value of V/U for which the total pressure at point B of a vortex chamber is just equal to the ambient pressure is plotted in figure 5 as a function of the length-to-diameter ratio of the chamber. Here again the Reynolds number N is an independent parameter. As one might expect, the lower the Reynolds number the higher must be the V/U of the vortex chamber to achieve the critical pressure drop. A very interesting fact in regard to these results is the extremely low ratio of V/U that is required to make a one-celled flow an impossibility for normal vortex chambers.

This is about all the information concerning the behavior of laminar solutions that it will be useful to present at this time. Since we will be primarily interested in turbulent vortices, we will proceed to a short discussion of how we might expect the results discussed above to be modified for the case of turbulent motion.

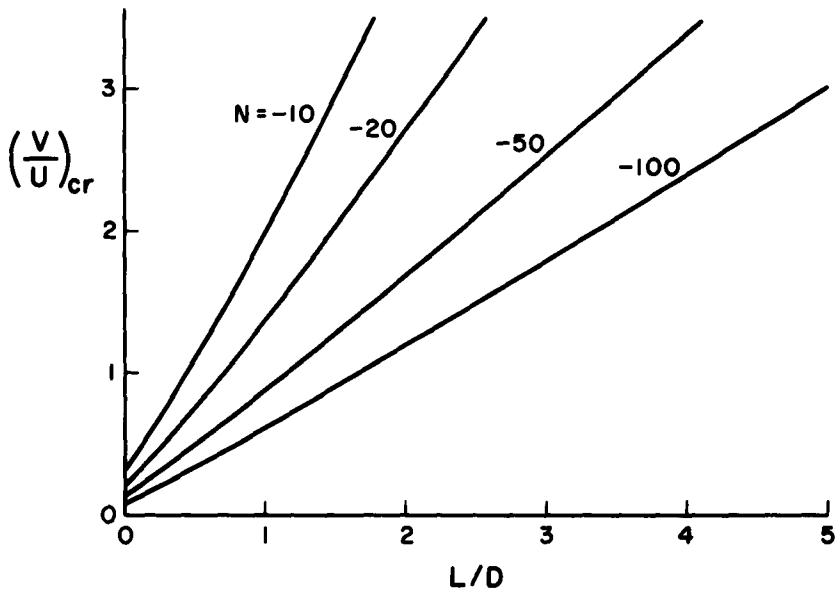

Figure 5. Dependence of $(V/U)_{cr}$ on L/D for several radial Reynolds numbers N based on the solutions of Donaldson and Sullivan.

4. Turbulent Vortices

At the present time, far too little is known concerning the nature of turbulent stresses in general or, for that matter, about turbulent stresses in the particular case of the vortex chambers under discussion here to permit an analytical solution to equations (10) through (13). However, if one assumes a typical mixing length formulation for the turbulent stresses either of the form

$$-\rho\overline{\tilde{u}'\tilde{v}'} = \rho\ell^2\left|\frac{\partial\tilde{v}}{\partial\tilde{r}} - \frac{\tilde{v}}{\tilde{r}}\right|\left(\frac{\partial\tilde{v}}{\partial\tilde{r}} - \frac{\tilde{v}}{\tilde{r}}\right) \tag{16}$$

or

$$-\rho\overline{\tilde{u}'\tilde{v}'} = \rho\ell\Delta\tilde{v}_{max}\left(\frac{\partial\tilde{v}}{\partial\tilde{r}} - \frac{\tilde{v}}{\tilde{r}}\right) \tag{17}$$

and similar expressions for the other stresses, it is not hard to show that the very simple flows of the form

$$\begin{aligned} u &= u(r) \\ v &= v(r) \\ w &= zf(r) \end{aligned} \tag{18}$$

obtainable in the laminar case can no longer identically satisfy the equations of motion. Because of this difficulty, as well as the conceptual difficulties inherent in applying a mixing length or other empirical approach, no theoretical analyses similar to that given by Donaldson (1961) and pursued by McCune and Williamson (1961) have been attempted.

Actually, in practice, the turbulent motions observed can come very close to satisfying the conditions given in equations (18). Thus, from a practical point of view,

some insight into the behavior of turbulent vortices can be gotten by considering them to behave in a manner similar to laminar vortices. In this case, however, to describe the viscous effects we replace the Reynolds number UR/ν by a number proportional to U/V. That is for turbulent vortices, we take an effective Reynolds number N^* defined as

$$N^* = k \frac{U}{V} \tag{19}$$

As mentioned before, this reduces the number of parameters governing the vortex motions under consideration to just one, namely, U/V. What, then, would we expect to find in regard to the behavior of such parameters as are plotted in figures 4 and 5 for the case of turbulent vortices. Since there is only one parameter, the families of curves dependent on Reynolds number for both the one-celled and two-celled flows plotted in figure 4 would collapse into just one curve for each family. Further, since the critical rotational speed $(V/U)_{cr}$ as shown in figure 5 is no longer a function of Reynolds number, we would expect to find that $(V/U)_{cr}$ is a function of L/D alone. In view of this fact, we would expect, for a given vortex chamber, that a pressure plot such as that shown in figure 4 would also consist of just a single curve. This curve would start out from $V/U = 0$ following the single curve of pressure versus V/U for one-celled vortices. As it approached some critical value of V/U, the curve would transit so as to follow the curve of pressure versus V/U for two-celled vortices. While following the pressure curve for any one particular type of flow (one-celled or two-celled), we would expect these curves to have less negative slope than the curves of constant Reynolds number

since we are effectively increasing the viscous action or lowering the effective Reynolds number as V/U is increased.

Before passing on to a discussion of experimental results, it is worthwhile to point out an interesting constraint on the total physical stress $\tau^*_{r\phi}$ in a vortex, whether it is laminar or turbulent, for the special case for which the tangential velocity is a function of the radial coordinate alone. In this case, the equation governing the tangential velocity, equation (12), may be written in terms of the total stress

$$\tau^*_{r\phi} = \mu \left(\frac{\partial \tilde{v}}{\partial \tilde{r}} - \frac{\tilde{v}}{\tilde{r}} \right) - \rho \overline{\tilde{u}' \tilde{v}'} \tag{20}$$

as

$$\frac{\partial}{\partial \tilde{r}} (\tilde{r}^2 \tau^*_{r\phi}) = \rho \tilde{u} \tilde{r} \frac{\partial}{\partial \tilde{r}} (\tilde{r} \tilde{v}) \tag{21}$$

Integrating equation (21) and noting that $\tau^*_{r\phi} = 0$ at $\tilde{r} = 0$ one obtains

$$\tau^*_{r\phi} = \rho \tilde{u} \tilde{v} - \frac{\rho}{\tilde{r}^2} \int_0^{\tilde{r}} \tilde{r} \tilde{v} \frac{\partial}{\partial \tilde{r}} (\tilde{r} \tilde{u}) d\tilde{r} \tag{22}$$

Thus the total stress and hence the Reynolds stress can be determined from a measurement of the mean velocity profiles u and v. This relationship is often useful in considering the flow within turbulent vortices (see for example Donaldson (1961) and McCune and Williamson (1961)).

5. Experimental Apparatus

In order to check experimentally the nature of the cellular structure of simple vortices such as have been discussed above, an apparatus was constructed that was designed specifically to be able to test the conjectures put forward in the preceding sections.

5.1. Vortex chamber

The chamber used to produce the desired three-dimensional vortex flows was designed so as to provide the greatest flexibility in establishing the various boundary conditions of interest. The vortices were produced inside a rotating tube of uniformly porous ceramic material 11-1/2 inches long, with an inside diameter D of 2.2 inches and a 3/16-inch wall thickness. This tube was supported vertically between end plates, which, in turn, were mounted on the inner races of a pair of ball bearings. The bearing outer races were held in fixed end plates which also acted as end covers for the steel plenum chamber surrounding the rotating assembly (see figure 6). A highly effective labyrinth seal was machined in each rotating and stationary end plate to minimize the leakage. The tube was rotated by means of a belt-driven pulley attached to the lower rotating end plate. A 3/4-horsepower direct current motor was used to drive the assembly. The power supply was a variable voltage, rectifier type which made possible rotational speeds up to 2400 rpm. For the 2.2-inch tube used, a maximum tangential wall velocity of about 24 ft/sec could thus be obtained. Air was supplied from a 100-cubic foot storage tank at 200 psig. An automatic, spring-loaded regulator valve was used to maintain the desired stagnation pressure in the plenum chamber. The highest working pressure

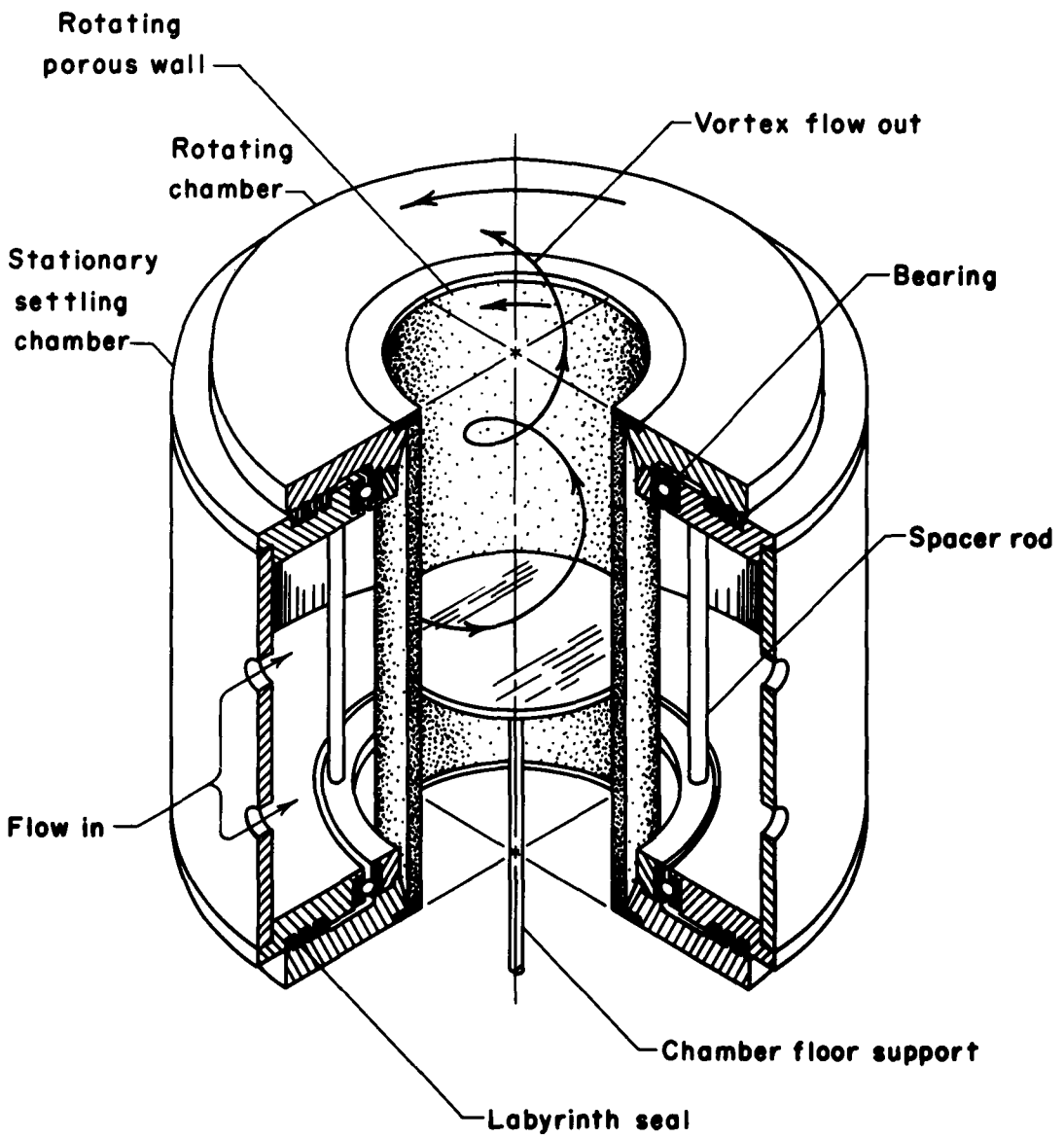

Figure 6. Cutaway view of vortex chamber apparatus.

generally used (about 3 psig) was found to give a radial velocity at the wall of about 6.5 ft/sec which corresponds to a radial Reynolds number $N = UR/\nu \approx -3800$.

The effective length L of the vortex "cup" was regulated by means of a movable floor plate inserted at the lower end of the tube. The axial position of this plate was adjusted by means of a motor-driven jack screw. The diameter of the plate was slightly less than the inside diameter of the tube so that no contact with the rotating tube was possible. The slight gap at the edge of the plate was judged to have little effect on flow conditions in the vortex cup. The maximum ratio of length to diameter L/D, using the 2.2-inch tube, was slightly over 5.

The entire apparatus--vortex chamber, regulator, drive motor, and jack screw assembly--was mounted in a rigid steel frame which provided convenient mounting locations for necessary instrumentation (see figures 7 and 8).

The device just described was thus capable of establishing vortex-type flows within the porous tube for any tangential velocity up to 24 ft/sec, any radial Reynolds number up to -3800, and for any length-to-diameter ratio up to 5, with all three parameters independently variable.

5.2. Instrumentation

The radial pressure distribution at the bottom of the vortex was measured by means of six static pressure holes in the floor plate. Static pressure and total pressure on the center line for various axial locations ($0 < z/L \leq 1.0$) were measured by means of suitable tubes made of .032-inch O.D. stainless steel tubing and mounted either at the center pressure tap of the floor plate or from above. The most reliable performance was achieved with a dual probe having

Figure 7. Vortex chamber mounted in stand showing drive motor and chamber floor actuating assembly. The variable voltage direct current power supply is at the right.

Figure 8. View of vortex apparatus showing porous cylinder and 5-hole prism type probe in position.

separate static and total pressure tips each of which could be positioned in the region of interest by rotating the tube 90° about its axis--the probe axis being normal to the vortex axis. This probe was mounted above the chamber and its use was limited to positions near the top of the vortex cup.

Velocity profile measurements were made with two commercially available, pitch and yaw sensitive, calibrated probes. Each was of the 5-hole type, one having a prism tip and the other a conical tip. The diameter of each probe at the tip was .12-inch. (Factors influencing the use of such probes in shear flows are discussed in Section 6.) The prism probe was used for velocity distributions both at the top of ($z/L = 1.0$) as well as inside the vortex cup. The conical probe was used only at the top.

All pressures were read from an adjustable-tilt alcohol manometer consisting of four U-tubes suitably connected to the probes.

5.3. Calibrations

Measurement of the supply tank blowdown rate, assuming constant tank temperature, was used to determine the approximate mass flow rate as a function of plenum chamber pressure. The leakage flow through the labyrinth seals was determined with a solid tube in place of the porous tube, and this flow was subtracted from the over-all mass flow to determine the net flow through the porous wall. The leakage rate was found to be less than 1 per cent of the total for all conditions tested. The over-all mass flow was independent of both rotational speed and length-to-diameter ratio of the vortex cup, so that a single calibration curve was sufficient for all possible conditions. Values of U and N were based on this curve assuming a uniform axial distribution of mass flow through the porous wall. Rotational speed was calibrated as a function of drive motor armature voltage by means of a Strobotac.

6. Experimental Results

Since the principal objective of this work was the establishment of criteria for determining the type of cellular structure of vortices, procedures for detecting the existence of such structure were first developed. Assuming that for a radial inflow the only possible structures have either one or two cells, as indicated by the laminar theory, two methods of detecting such structure were tried: (1) measurement of static and total pressures on the center line and (2) direct measurement of component velocity profiles.

6.1. Static and total pressures on the center line

As defined herein, a two cell vortex with radial inflow at the outer boundary (porous wall) must consist of a peripheral region of upward axial flow (directed out of the top of the vortex cup) and a central region of downward axial flow (directed into the vortex cup). The upward axial flow region thus consists of fluid that entered radially at the outer boundary plus the fluid that entered axially at the center and ultimately reversed its direction. (For an axially symmetric flow, of course, radial and tangential velocity components must vanish at the center.) Detection of a two-celled flow was thus based on the presence of either a zero or negative (downward) axial velocity on the center line--zero axial velocity indicating the lower extremity of the center cell.

Total head tubes mounted at the bottom of the vortex chamber facing upward in an axial direction and tubes mounted from above facing downward were used in conjunction with similarly mounted static tubes to make extensive pressure surveys for a range of radial Reynolds number N, tangential wall velocity V, length-to-diameter ratio L/D,

and centerline locations $\tilde{z}/L$. Equality of total and static pressures so measured under identical boundary conditions was assumed to be indicative of zero axial velocity. Consistent results, however, were difficult to achieve in this way because the necessary exact matching of boundary conditions for corresponding total and static pressure measurements made during separate runs was extremely difficult. Subsequent use of the dual probe described earlier resulted in more reliable data since the total and static pressures at the same point were measured at very nearly the same instant. This probe was used to measure the outward axial component of total pressure as well as the static pressure on the center line at $\tilde{z}/L = 1.0$ for various values of the parameters.

With L/D and N held constant, readings were taken for a number of tangential velocities V. Typical results are shown in figures 9, 10, 11, 12, and 13 for several radial Reynolds numbers and several depth-to-diameter ratios. The data are presented in the form of a pressure coefficient based on radial dynamic pressure at the wall plotted against the non-dimensional velocity ratio parameter V/U. For very small tangential velocities, it is seen that the difference between the two curves represents the dynamic pressure due to the upward (positive) axial velocity on the center line. As V is increased, there is a drop not only in the static and total pressures, but also in the difference between them. This convergence is indicative of a decreasing upward axial velocity on the center line. Finally, the two pressures become equal, at which point the upward axial velocity is apparently zero. Further increase of V/U beyond $(V/U)_{cr}$ shows evidence of a downward axial velocity. With the total head tip of the probe still facing downward, it begins to register pressures slightly but consistently less than does the static tip.

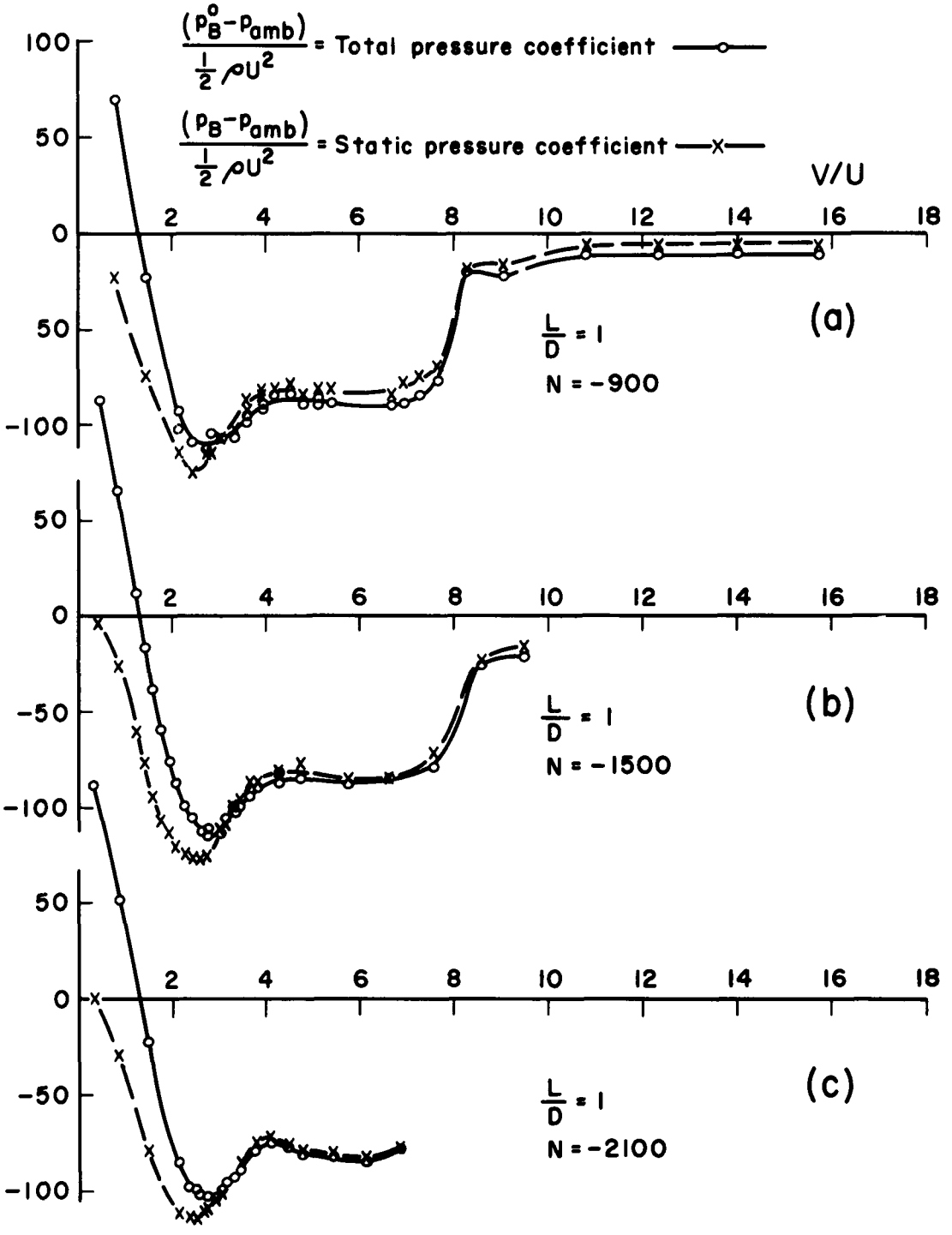

Figure 9. Total and static pressures at the center of the exit plane (point B) as functions of V/U.

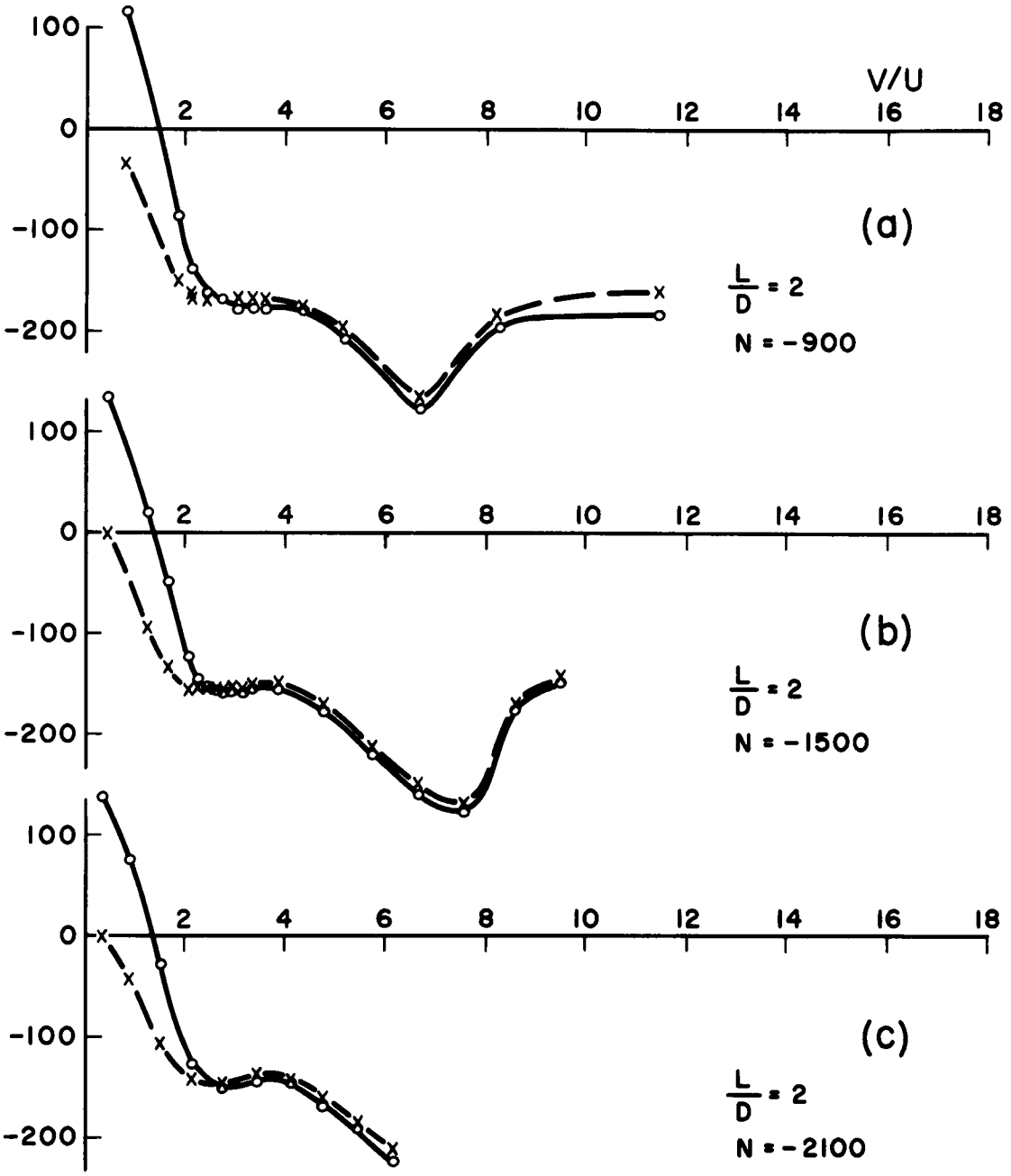

Figure 10. Total and static pressures at the center of the exit plane (point B) as functions of V/U.

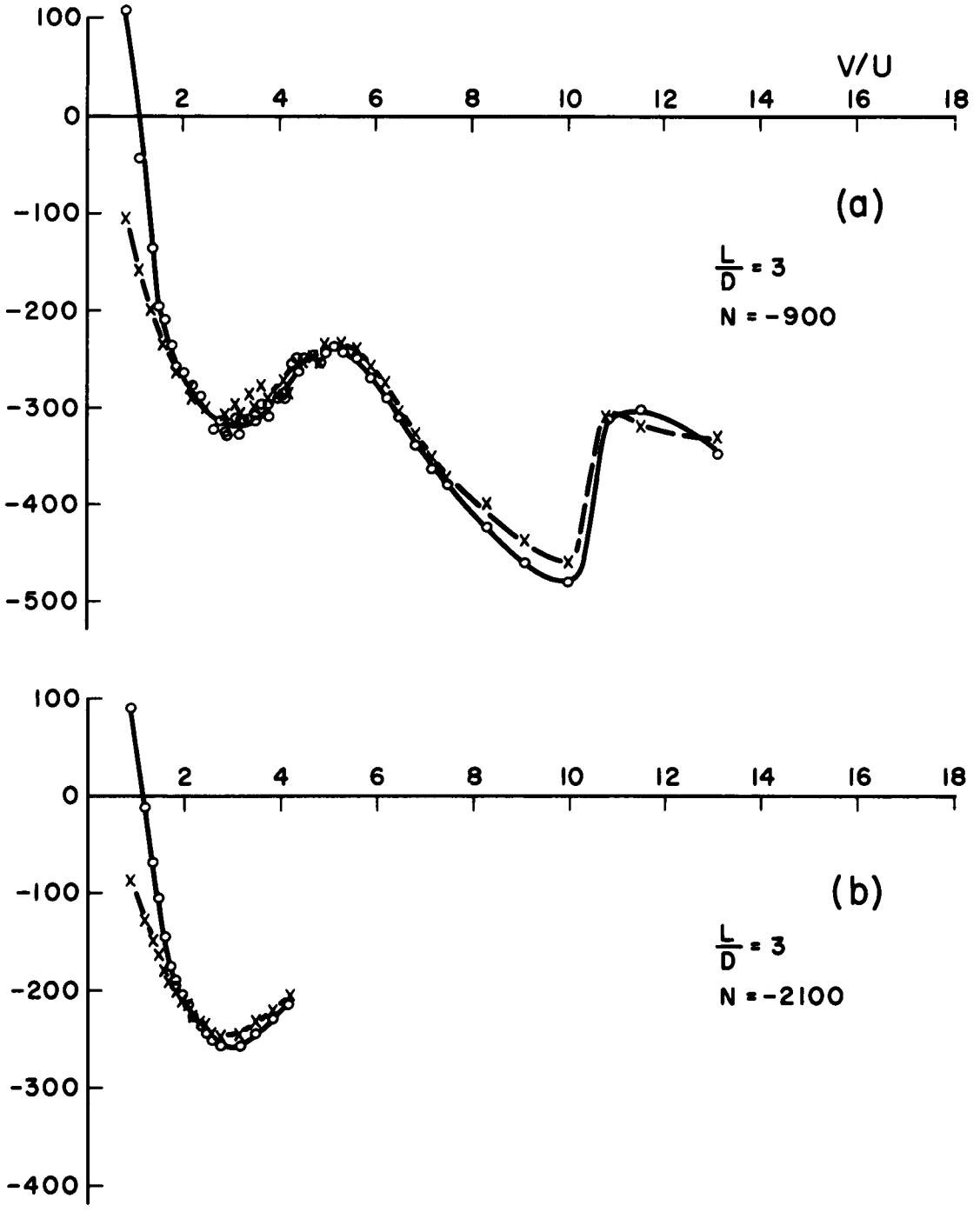

Figure 11. Total and static pressures at the center of the exit plane (point B) as functions of V/U.

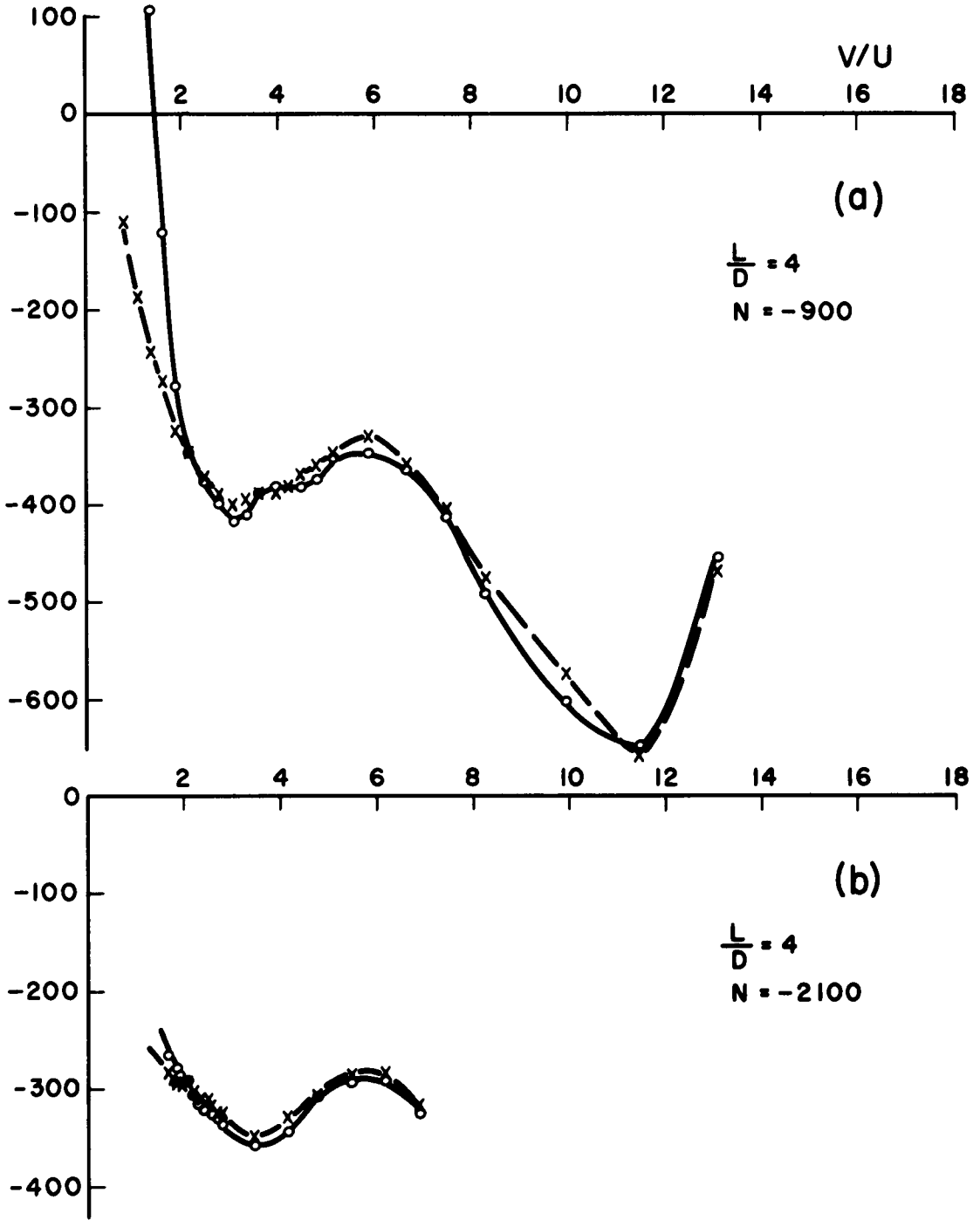

Figure 12. Total and static pressures at the center of the exit plane (point B) as functions of V/U.

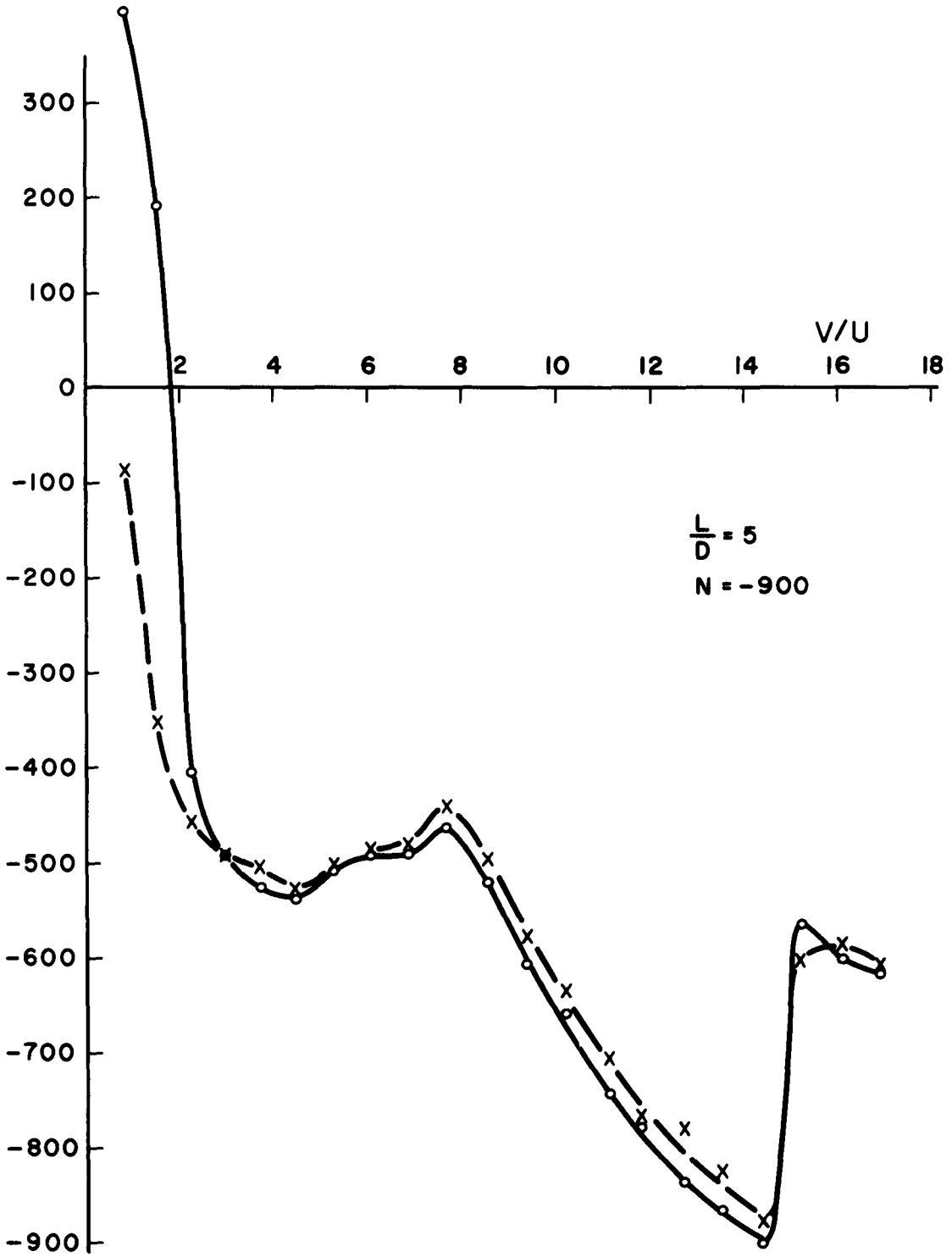

Figure 13. Total and static pressures at the center of the exit plane (point B) as functions of V/U.

This is what one might expect if the total head tube were now considered to be sensing a base pressure due to the axial flow directed away from its open end. This condition persists to the highest V/U possible. The few cases where individual points are reversed all occur in the vicinity of the peculiar region of sudden pressure rise and are therefore attributed to the difficulty of maintaining steady flow conditions in this region.

In all the above cases, for a given cup length-to-diameter ratio L/D, the value of $(V/U)_{cr}$ was found to be virtually independent of radial Reynolds number over the range tested. The dependence of $(V/U)_{cr}$ on L/D is shown in figure 14 with the values of N indicated. The significance of the various features of figures 9 through 14 is discussed in section 7.

6.2. Velocity profiles

Typical tangential and axial velocity profiles for one of the cases just discussed (N = -900, L/D = 5) are shown in figure 15. These profiles were determined by using the 5-hole conical probe mounted above the vortex chamber. Certain considerations involving probe effects on the accuracy of these profiles are discussed later in this section.

As V/U is increased, a decrease in outward axial velocity near the center is immediately apparent while the outer portions of the profile are essentially unchanged. The tangential profile at first exhibits increasing velocities near the center, but the maximum value soon begins to drop with increasing V/U while at the same time the radial location of the maximum is displaced outward. These trends continue until an inward axial velocity on the center line approximately equal to the maximum outward value is achieved. For higher V/U, the maximum inward velocity changes only slightly while the radial extent of the inner cell increases until it finally occupies a large portion

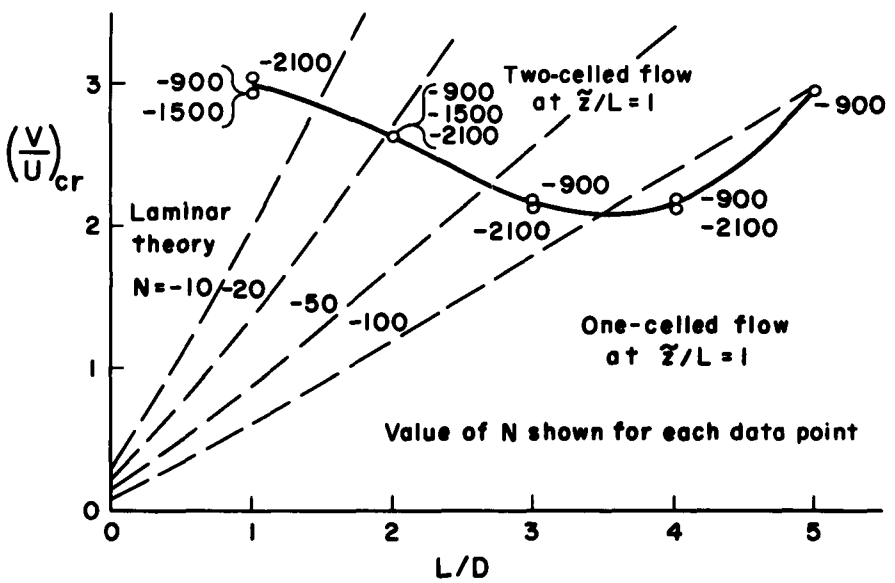

Figure 14. Variation with L/D of measured values of $(V/U)_{cr}$ at point B ($\tilde{z}/L = 1$).

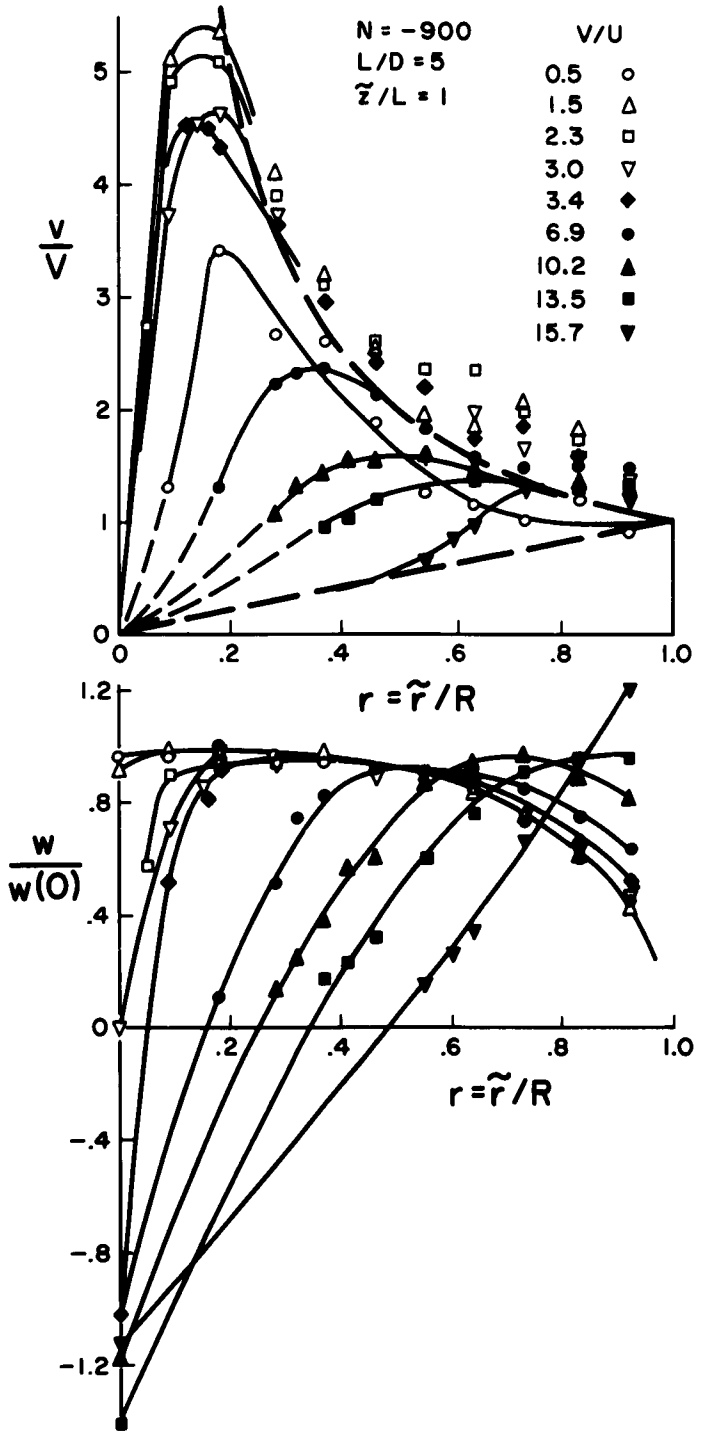

Figure 15. Tangential and axial velocity profiles measured in the exit plane with the conical tip probe. Inviscid and solid-body rotation tangential profiles are shown by heavy dashed lines.

of the 2-celled system.

Since it was not possible to measure negative w directly with the 5-hole conical probe, those values shown on the center line are computed from the static pressures measured with the dual probe, assuming a total pressure equal to atmospheric. Positive values of w on the center line measured with both probes showed excellent agreement except in the sensitive region near w = 0.

6.3. Probe effects on velocity measurements

By far the most significant source of experimental error is thought to lie in the use of the 5-hole probes in regions of high shear and near solid boundaries.

A description of the operation of the 5-hole conical probe is now given in order to clarify the discussion of such probe error sources. This probe had a single "total head" hole at the apex of the concial tip with 4 "static" holes a short distance down the conical surface, the latter being spaced 90° apart and equidistant from the apex. One opposed pair of static holes was aligned laterally with respect to the probe shaft and the other pair longitudinally. The probe was mounted with respect to the vortex chamber as shown in figure 16. It could be traversed radially in either of two directions so that either pair of holes could be in radial or tangential alignment. In order to determine the local flow direction, at a particular radial location, the probe was rotated about its shaft until equal pressures were registered by the lateral holes. In this position, the probe lay in a plane containing the apparent velocity vector. The angle between the probe and the velocity vector was then determined from the calibrations

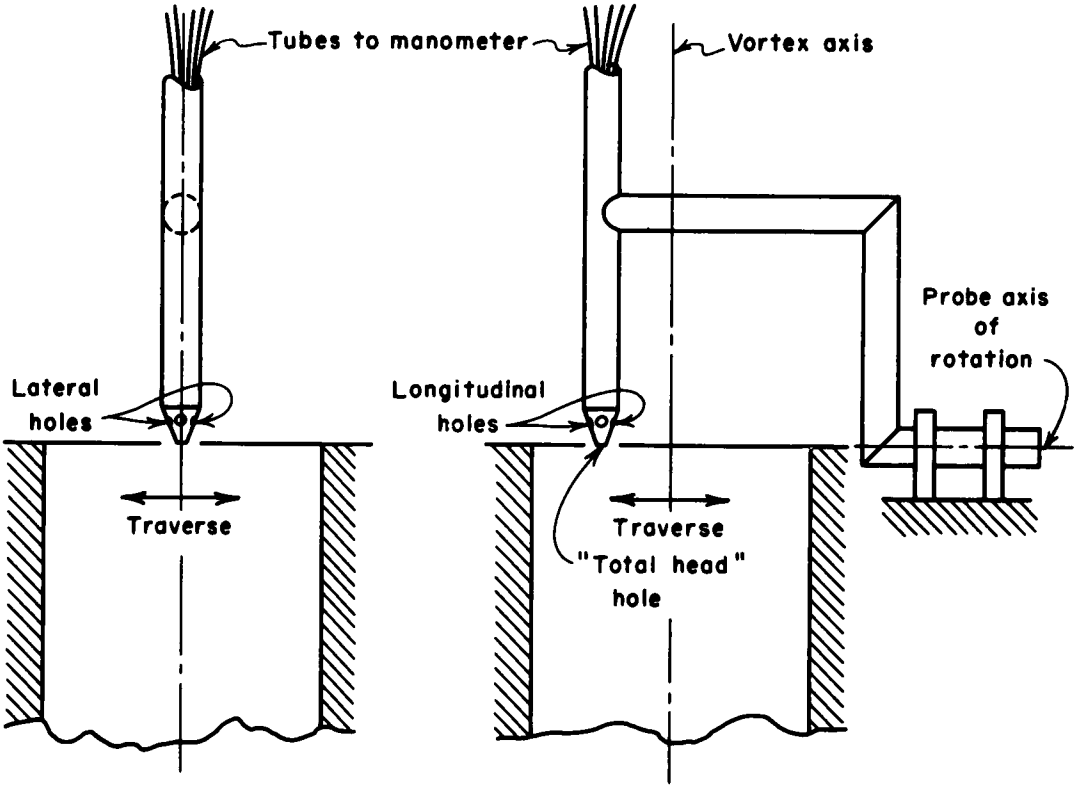

Figure 16. Schematic views of conical tip probe mounting arrangement. Transverse travel (traverse) is indicated on the left and axial travel on the right.

by measuring the pressure difference between the longitudinal holes. Calibrations also gave the true total pressure corresponding to the "total head" hole reading for that angle. True dynamic pressure was similarly calibrated for the difference between lateral hole "static" pressure readings and "total head" hole readings as a function of the angle. With the magnitude and direction of the velocity vector so determined, the components were computed. When used in this way in flows with regions of high shear, it is clear that misleading data may easily result since holes on opposite sides of a symmetrical body immersed in a shearing flow will show a pressure difference. Near solid boundaries, too, there is a distortion in the flow pattern around the probe due to an interference-type effect which also changes the angle at which the flow approaches the probe. A third consideration is the radial static pressure gradient balancing the centrifugal force. The finite radial distance between the radially oriented pair of holes may be sufficient to sense this gradient and thus affect the accuracy still further. A full quantitative evaluation of all these factors and how they interact and depend on probe orientation for a particular flow would require estensive tests with the probe immersed in flows whose properties were determined in some alternate manner. Such tests would represent a sizeable experimental program in themselves and so none have been attempted. Application of existing boundary correction procedures to probe data in this case was felt to be of little value. However, it is possible to draw some general conclusions about the validity of the measured profiles.

Tangential velocity. Effects due to high shear should depend on whether the lateral or longitudinal holes are used to evaluate this component. Check runs (figure 17) using both methods seem to bear out the reasoning that the

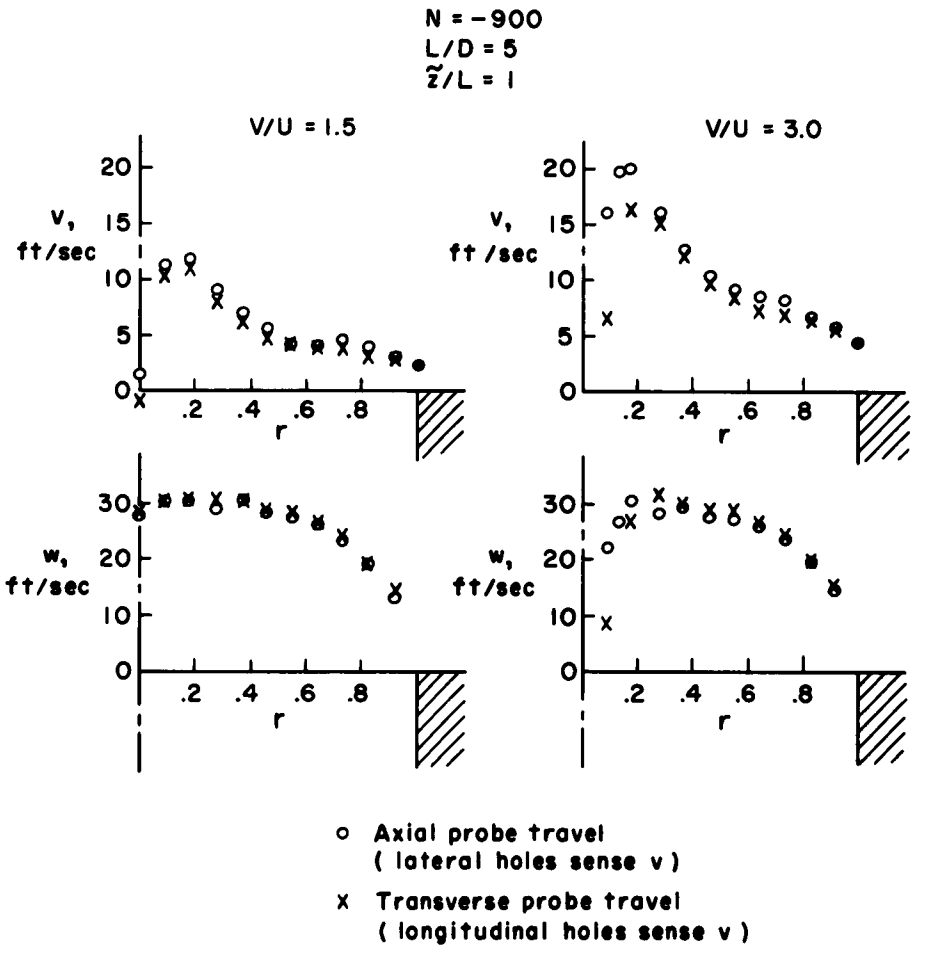

Figure 17. Comparison of tangential and axial velocity profiles using both probe traverse methods.

longitudinal holes may give lower values than the lateral holes. On the other hand, the solid-boundary interference effect could be appreciable. Even at a distance of 3 or 4 probe diameters from the wall (outer 40 per cent of the profile), such an effect could be felt. Again, the method of measurement should be a factor. It appears quite consistent, therefore, to reason that the outer portions of the v profiles shown in figure 15 exceed the inviscid profile due to wall effects on the probe. It is also consistent to note that the check runs using the longitudinal holes to determine v gave lower values in this region.

Axial velocity. A higher degree of precision in measuring axial velocity components appears to be inherent in either method of measurement except in regions where the tangential component is of comparable magnitude. The close agreement shown by the check runs appears to bear this out.

Radial velocity. Although, as has just been discussed, it is extremely difficult to measure tangential and axial velocities with any great degree of precision, the measurements are reasonably reliable quantitatively and are certainly accurate enough to give qualitatively the behavior of these profiles with variations of the basic parameters. On the other hand, since the radial velocities that must be measured in such vortices are an order of magnitude smaller than the other velocity components, the measurements that were made of these velocities are probably of very little value even in a qualitative sense. Nevertheless, for completeness, as well as to give some idea as to the magnitude of the experimental errors that were involved in the measurement of the velocity component profiles, a typical measurement of radial velocity is shown in figure 18. Included in this figure for comparison with the local measurements are the radial velocity at the wall as obtained

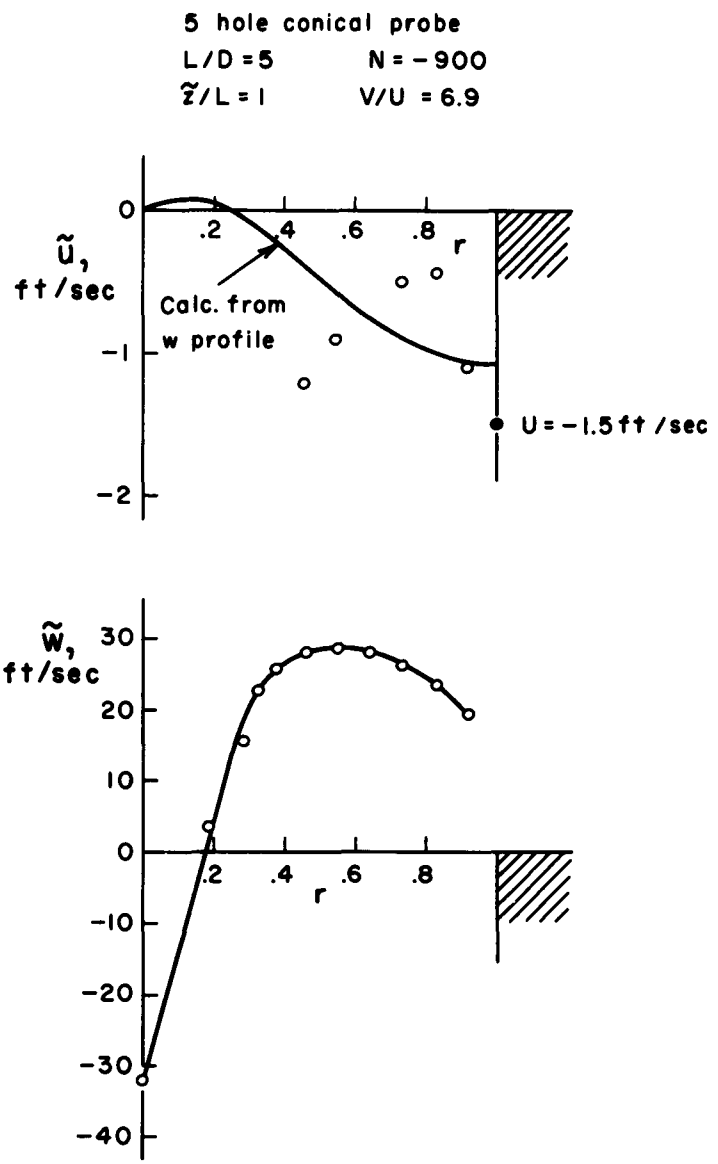

Figure 18. Typical radial velocity measurements compared with the profile computed from the measured axial velocity distribution.

by mass flow measurement (the solid symbol) and a curve showing an estimate of what the actual character of the radial velocity profile must be like. This estimate was made by assuming that the axial velocity actually satisfied the equation $w = zf(r)$ so that the radial velocity could be obtained from the measured axial velocity distribution through integration of the continuity equation. It is seen that, as might be expected, the order of magnitude of the radial velocity as measured is correct but the experimental errors are such that no information is contained in these data concerning the character of the radial velocity profiles.

6.4. Static pressure profiles

In order to complete the picture of the behavior of flows in simple cylindrical vortex chambers, there are presented in figures 19 and 20 data concerning the static pressures within a typical vortex. Figure 19 shows typical plots of the non-dimensional pressure distributions obtained across the exit of the vortex as the parameter V/U is varied for the specific case when $L/D = 5$ and $N = -900$. Figure 20 shows for the same case a comparison of the static pressure at $\tilde{z}/L = 0$ and at $\tilde{z}/L = 1.0$ on the axis of symmetry as a function of V/U. It is interesting to note the change in the character of the static pressure distributions as V/U is increased above $(V/U)_{cr}$, which in this case is 2.95, and as V/U is increased beyond a second critical value at $V/U \approx 15$ where a jump in the static pressure on the centerline takes place for $\tilde{z}/L = 1$.

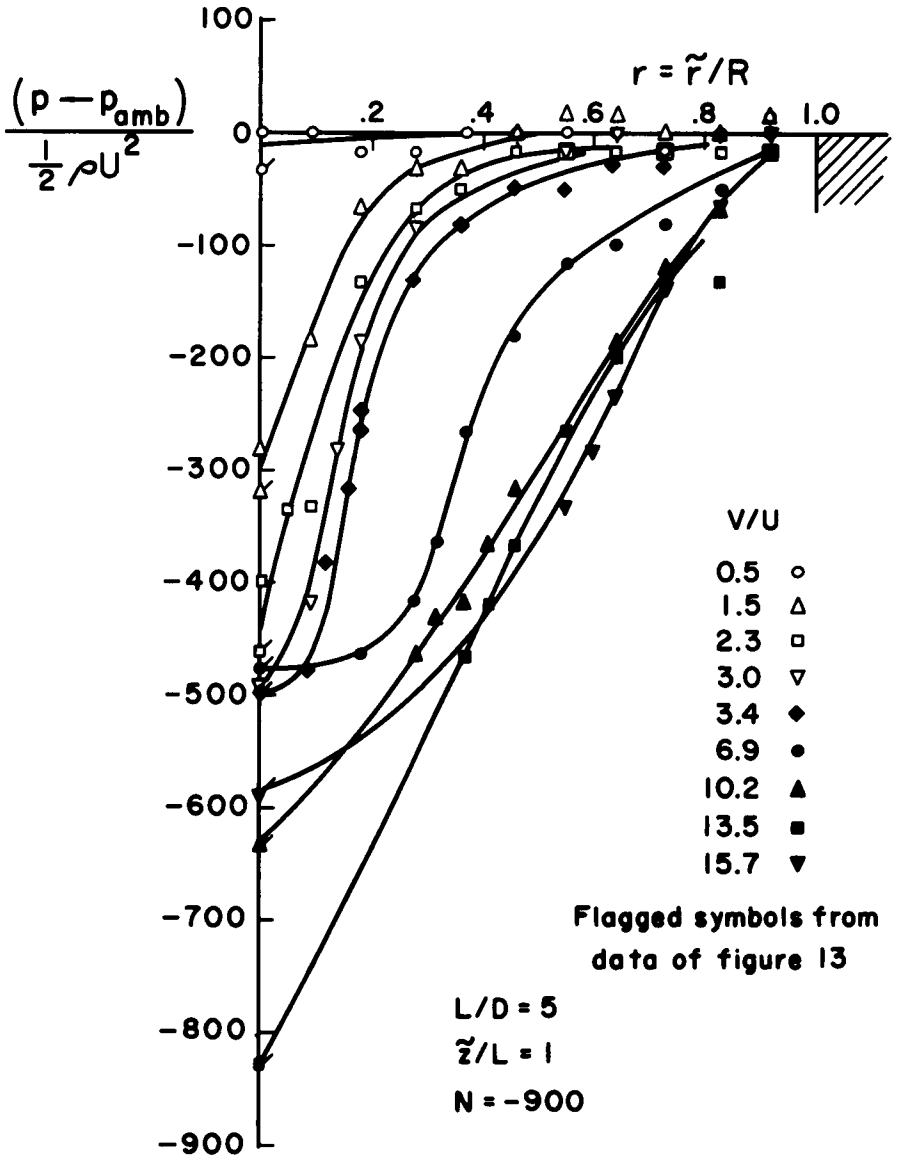

Figure 19. Measured static pressure distributions across the exit plane ($\tilde{z}/L = 1$).

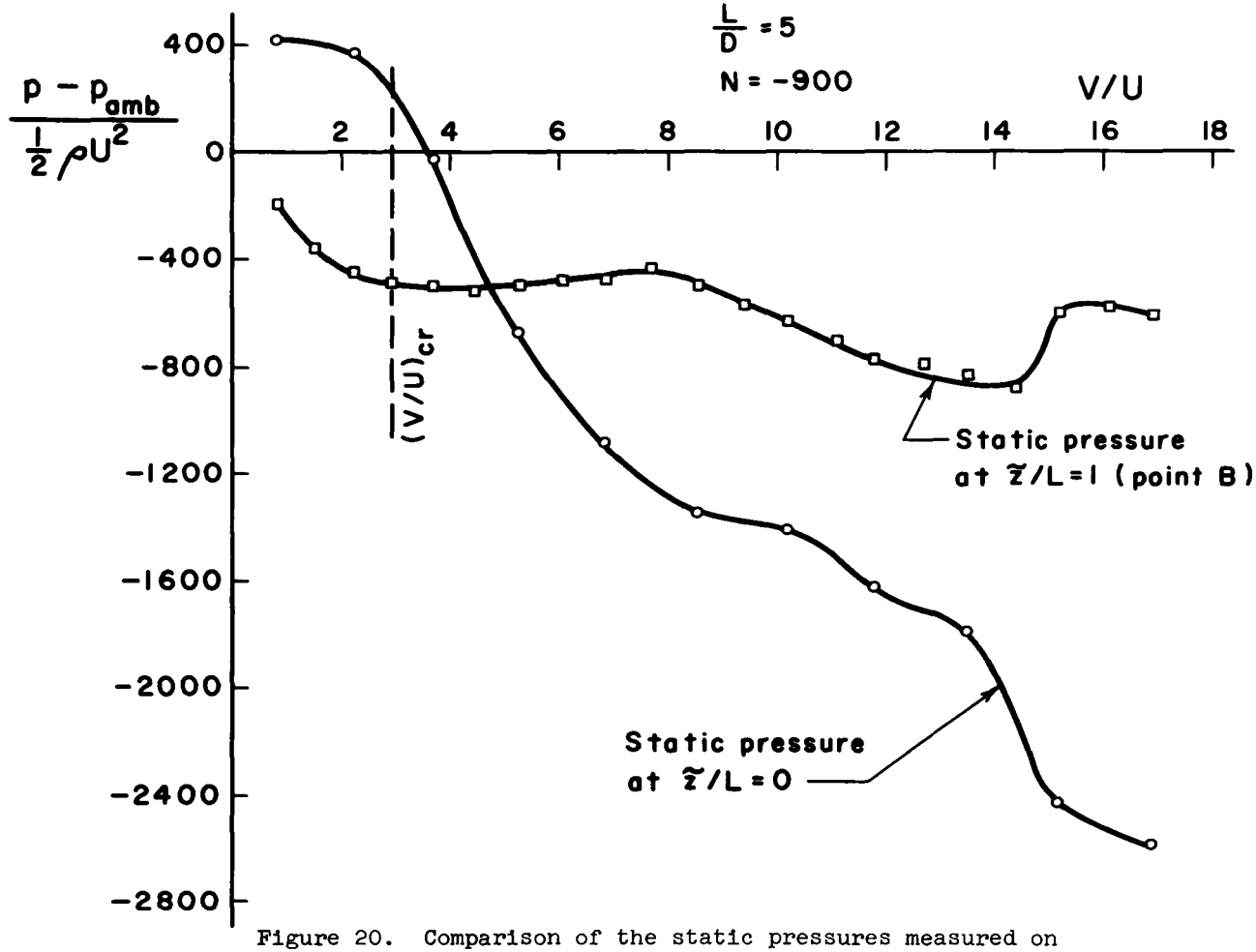

Figure 20. Comparison of the static pressures measured on the center line at the bottom ($\tilde{z}/L = 0$) and top ($\tilde{z}/L = 1$) of the vortex cup as V/U is varied.

7. Discussion of Experimental Results

The detailed behavior of the vortices on which experimental data have just been presented, especially the way in which these vortices form their second cell, can best be understood by means of a detailed discussion of a typical case. We will discuss in detail the vortex behavior for the case $L/D = 5$ and $N = -900$ with the aid of figures 21 and 22. Figure 21 consists of the data already plotted in figure 13, together with the following additional information: (1) theoretical curves for $(p - p_{atm})/\frac{1}{2}\rho U^2$ versus V/U obtained from the laminar theory for one-celled (dash dot curves) and two-celled (dash double dot curves) vortex configurations; (2) the pressure drop that might be expected if the fluid at the exit of the vortex were turning as a solid body (dashed curve); and (3) the pressure drops that one obtains from an integration of the approximate radial momentum equation

$$\frac{d\tilde{p}}{d\tilde{r}} = \frac{\rho\tilde{v}^2}{\tilde{r}}$$

using the measured tangential velocity profiles at several values of V/U (indicated by the solid symbols). Figure 22 gives a pictorial representation of the behavior of the streamlines in and around the vortex chamber as the rotational speed of the chamber wall is increased. Also shown in this figure are the tangential velocity profiles, typical of each condition, in the exit plane of the vortex.

Let us follow the behavior of the vortex on figures 21 and 22 as V/U is increased from zero to the highest value at which measurements were made. Initially, when the tangential velocity is zero, the flow in the vortex cap is similar to that shown in figure 22a. The axial flow in

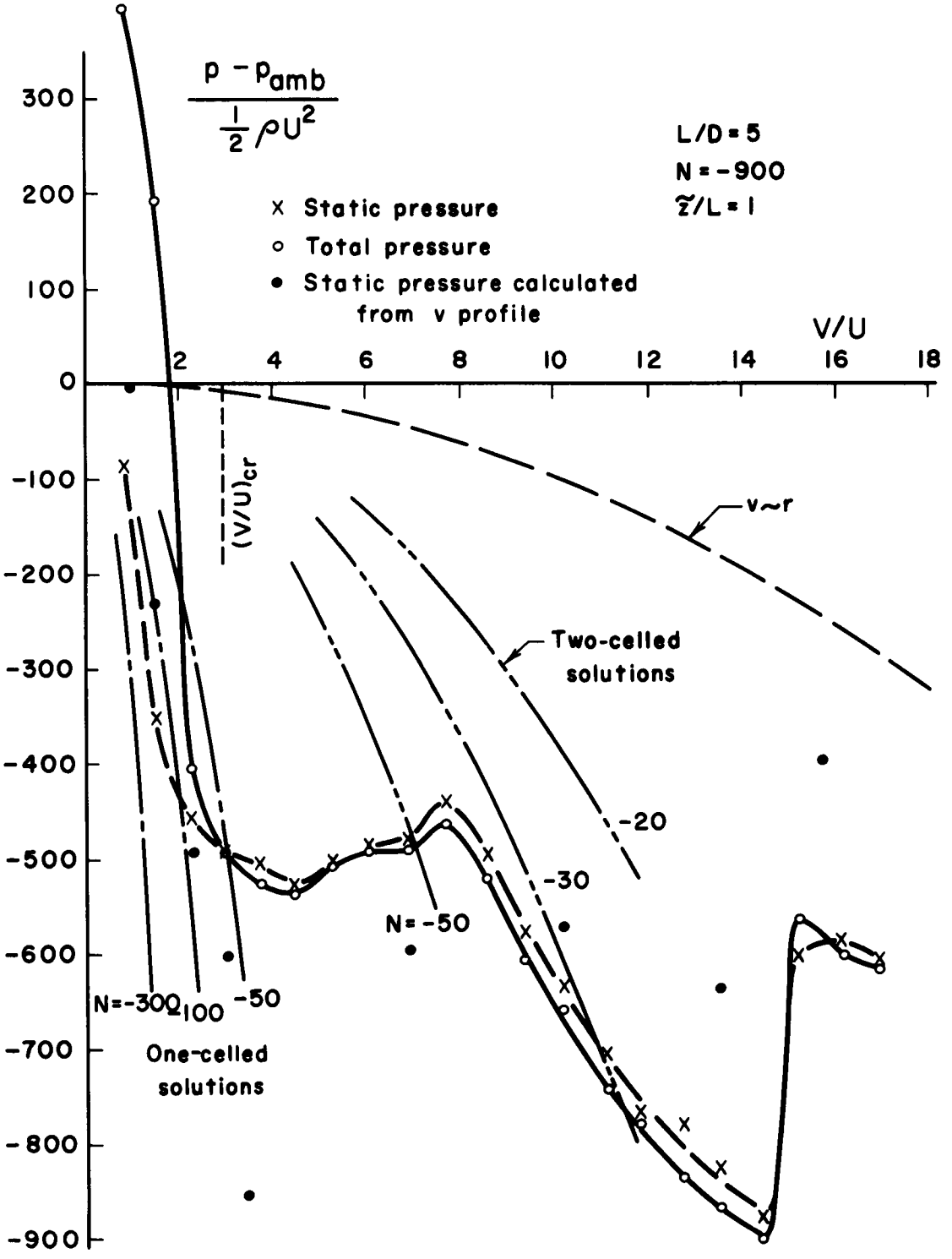

Figure 21. Comparison of measured pressure behavior at point B with that given by the laminar theory.

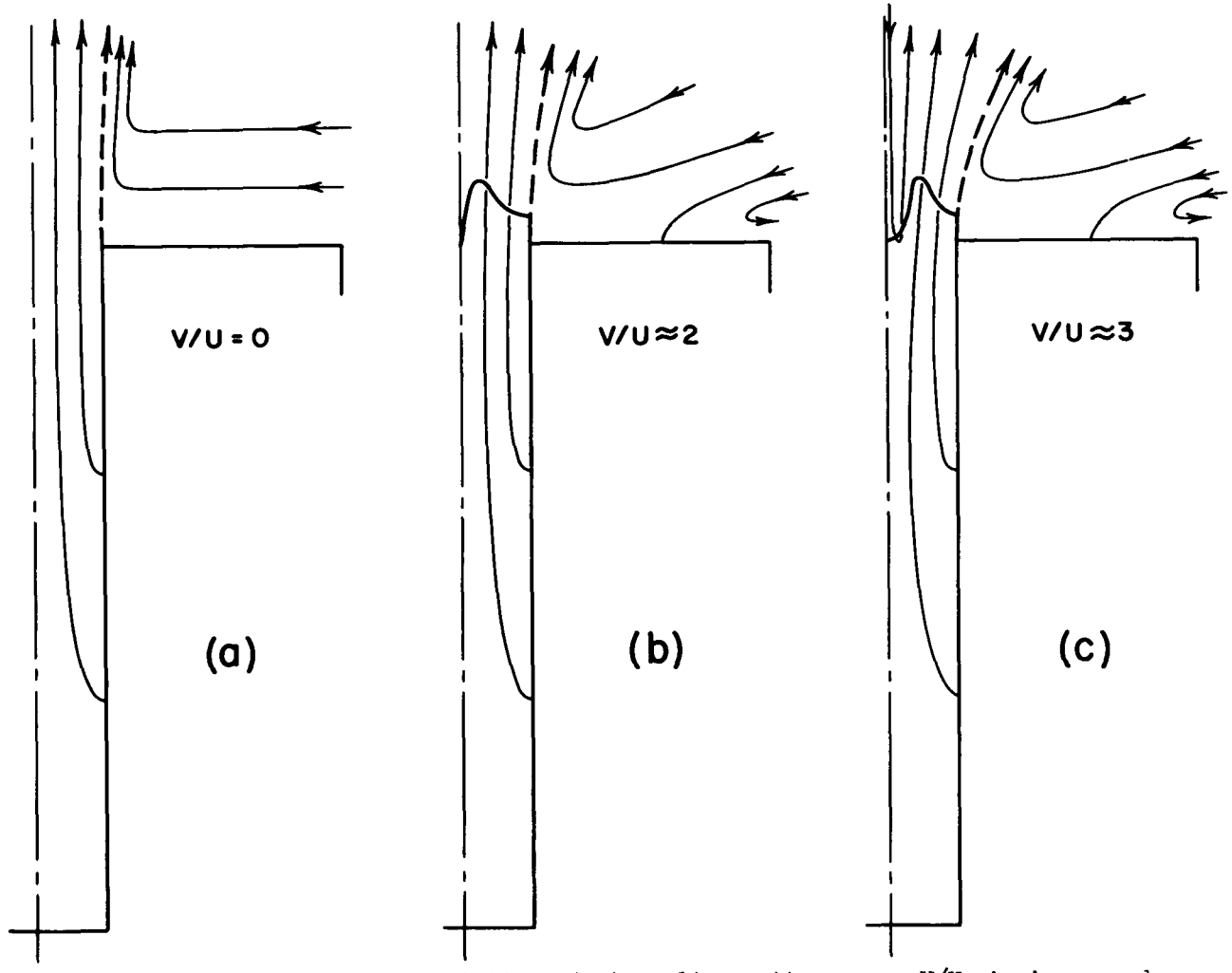

Figure 22. Pictorial representation of streamline patterns as V/U is increased. The approximate tangential velocity profiles are shown in the exit plane.

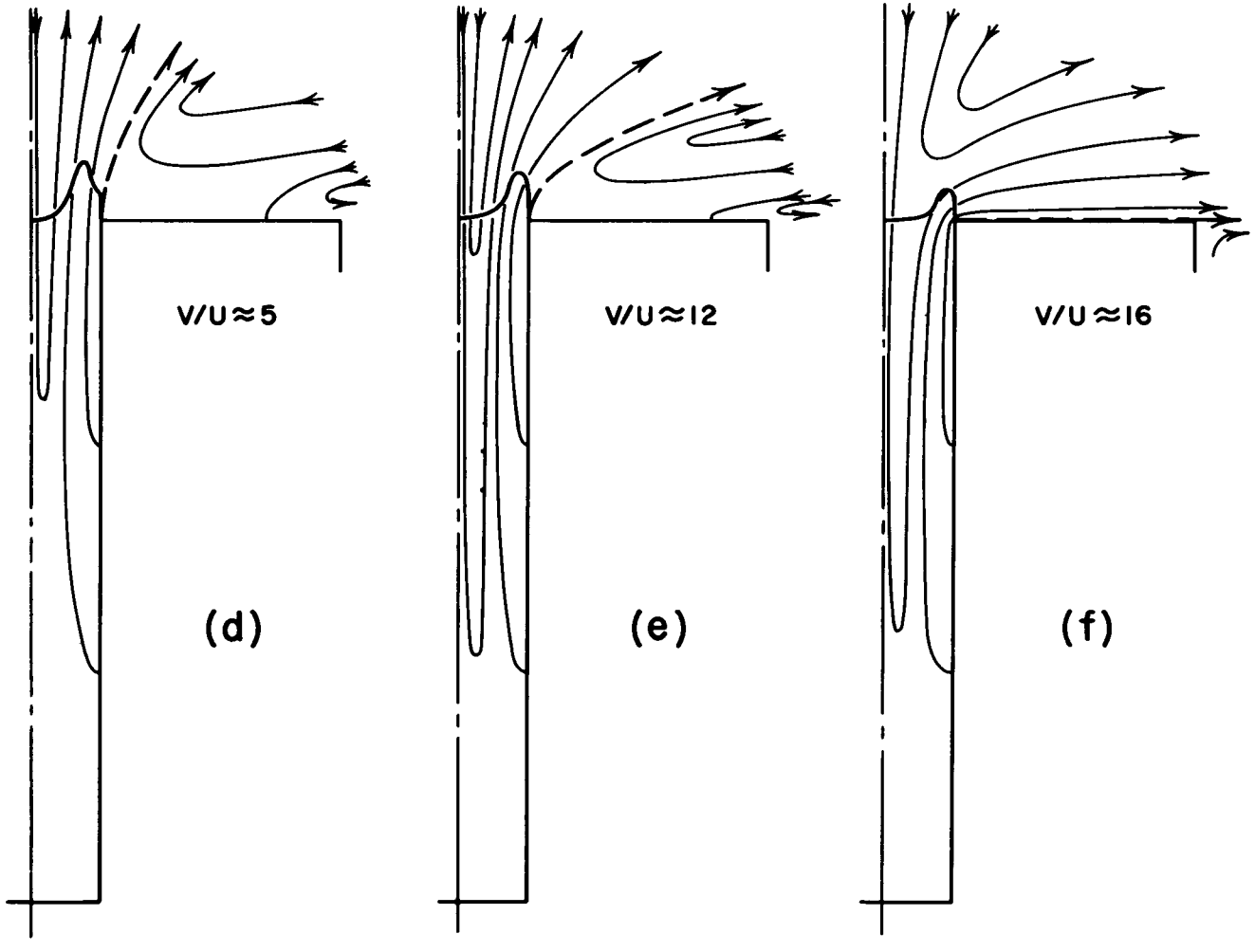

Figure 22 - concluded

the exit plane is everywhere outward with a velocity distribution that is very close to the theoretical curve for a one-celled laminar vortex, namely $\tilde{w}/\tilde{w}(0) = \cos(\tilde{r}/R)^2$. There is, to the scale of the static pressure plot shown in figure 21, essentially no difference between the static pressure on the vortex centerline in the exit plane and the ambient pressure (also see figure 19). The total pressure shown in figure 22 for $V/U = 0$ is higher than ambient pressure by just the dynamic pressure of the outgoing flow.

As V/U is increased from zero, the flow within the vortex cup retains its one-celled character as shown in figure 22b for $V/U \approx 2$. Nevertheless, the dynamic pressure of the exiting fluid on the centerline of the vortex is very rapidly reduced. This is evident both from figure 21 and from the actual $w/w(0)$ velocity profiles for this particular case which are shown in figure 15. Apparently, a second cell is forming somewhere high above the vortex chamber and is gradually moving towards the exit plane as V/U is increased.

We should also note in figure 22b that the entrained flow is no longer captured in just the same manner as it was when $V = 0$. This is due to the centrifugal pumping action of the rotating face plate of the vortex chamber. As a result of this pumping action, there is a stagnation point (actually a stagnation ring) somewhere on this rotating plate. The air above the streamline to this stagnation point is entrained by the flow out of the vortex chamber. The air below this streamline is forced outward away from the vortex by the pumping action of the face plate.

As the rotational speed is increased further, the dynamic pressure of the axial flow exiting from the vortex becomes less and less until at the critical value $(V/U)_{cr} = 2.95$ it is exactly equal to zero as shown in

figure 22c. We see that the second cell that had developed far from the vortex at low rotational speeds has been sucked down toward the vortex chamber until, at $V/U = 2.95$, the tip of this second cell has just reached the exit plane of the chamber. Up until this critical value of V/U, the tangential velocity distribution at the exit plane has not been greatly altered in character as may be seen from the tangential velocity distributions shown in figure 15. Thus, in the range $0 < V/U < (V/U)_{cr}$, the pressure on the centerline drops uniformly, roughly as the square of V/U.

Once the critical value of V/U has been reached, the character of the tangential velocity distributions in the exit plane changes markedly with V/U as the second cell of the vortex is sucked inside the chamber. Indeed, the tangential velocities are lowered so much in the center of the vortex (see figure 15) that the pressure drop is actually reduced somewhat as seen in figure 21. A typical streamline pattern for this regime is shown in figure 22d.

When the second cell of the vortex has been sucked completely into the vortex chamber, which occurs in the case under discussion at $V/U \approx 8$, the pressure drop across the vortex starts to increase again. It will be noted however that, instead of following a curve similar to those for constant Reynolds number as given by the laminar theory, the pressure drops far less rapidly. This behavior in all cases appears to be due to an effective increase in the turbulent or Reynolds stresses with increase in V/U as discussed in Sections 3 and 4. Streamlines typical of this flow regime are shown in figure 22e.

After the two-celled vortex pattern has been completely established, further increase in V/U results in a continued increase in the pressure drop across the exit of the vortex until a second critical value of V/U is reached. At this point, $V/U \approx 15$ in the case under discussion,

there is a rapid rise in the general level of pressure within the vortex at the exit plane. By careful probing of the flow external to the vortex cup with fine tufts and with smoke streams, it was possible to show that, in all cases, this pressure rise was associated with a rather sudden change in the flow pattern outside the vortex chamber. The nature of this change is shown in figure 22f. Inspection of the streamline patterns for $V/U < 15$ in figure 22 reveals that there is always an entrained flow. However, as V/U is increased, the streamlines leaving the vortex chamber do so in a more and more radial manner. It was found that at the second critical value of V/U the flow leaving the vortex cup attached itself almost immediately to the rotating face plate outside the vortex thus eliminating the entrained flow altogether. The spreading out of the streamlines outside the vortex that resulted was found to greatly reduce the amount of angular momentum that the fluid entering the second cell of the vortex could obtain by viscous action from the primary flow leaving the vortex. As a result of this lowering of the tangential velocity in the exit plane, the pressure drop across the vortex was greatly reduced.

It would be expected that since this change of streamline configuration must depend on the ratio of the general level of axial velocity leaving the vortex to V, the deeper the vortex chamber (higher $\overline{w}$) the higher would be the V/U required to effect this change. The fact that this is so and that all the vortex chambers investigated behaved in essentially the manner described above is amply demonstrated by figure 23 when all the static pressure measurements given in figures 9 through 13 are replotted.

It can be seen from figure 23 that since the vortex cup is shallow in the cases of small L/D, the air in the second vortex cell receives far less angular momentum from

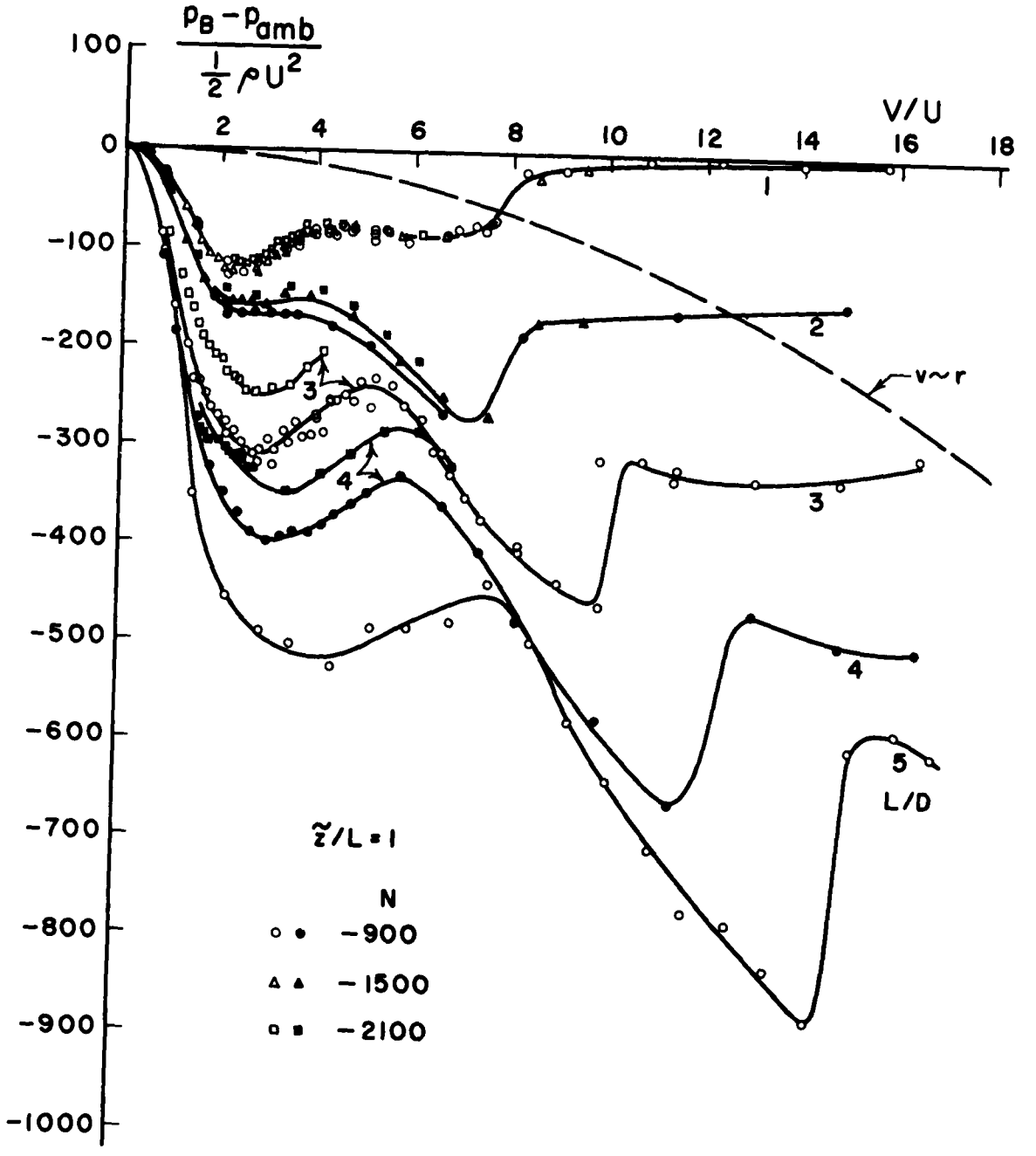

Figure 23. Summary of static pressure data as a function of V/U and L/D.

the primary vortex flow than in cases when L/D is large. This is particularly true for the case when L/D = 1 after the flow outside the vortex has attached to the rotating face plate (V/U > 8).

Another fact that is demonstrated by figure 23 is that V/U is the primary parameter governing the behavior of the vortices under discussion here. It will be noticed that for each vortex chamber tested (L/D varied), the results, though slightly dependent on Reynolds number are essentially controlled by the parameter V/U. This is particularly true of the vortex chambers of low L/D when the effects of molecular viscosity which are expected to be largest on the axial flow must necessarily be small.

The results shown in figure 23 as well as the basic measurements of $(V/U)_{cr}$ shown in figure 14, where it is seen that for all intents and purposes $(V/U)_{cr}$ is independent of Reynolds number for L/D < 5, give strong support to the basic conjectures of Sections 3 and 4 concerning the nature of turbulent vortices.

In this regard, it may be of some interest to determine the order of magnitude of the effective viscosity that a laminar flow (as given by the exact solutions of Donaldson and Sullivan) would have to have in order to match the static pressure drops that have been observed in the exit planes of the several vortex configurations tested. Figure 24 is a plot of the ratio of effective to molecular viscosity obtained by matching the experimental static pressure drops at the exit to those given by the laminar theory. This matching was only carried out when fully developed one- or two-celled vortex structures existed. The data are not, since the measured flows are not identical to those given by the laminar theory, of fundamental importance. Nevertheless, the general trend of the data

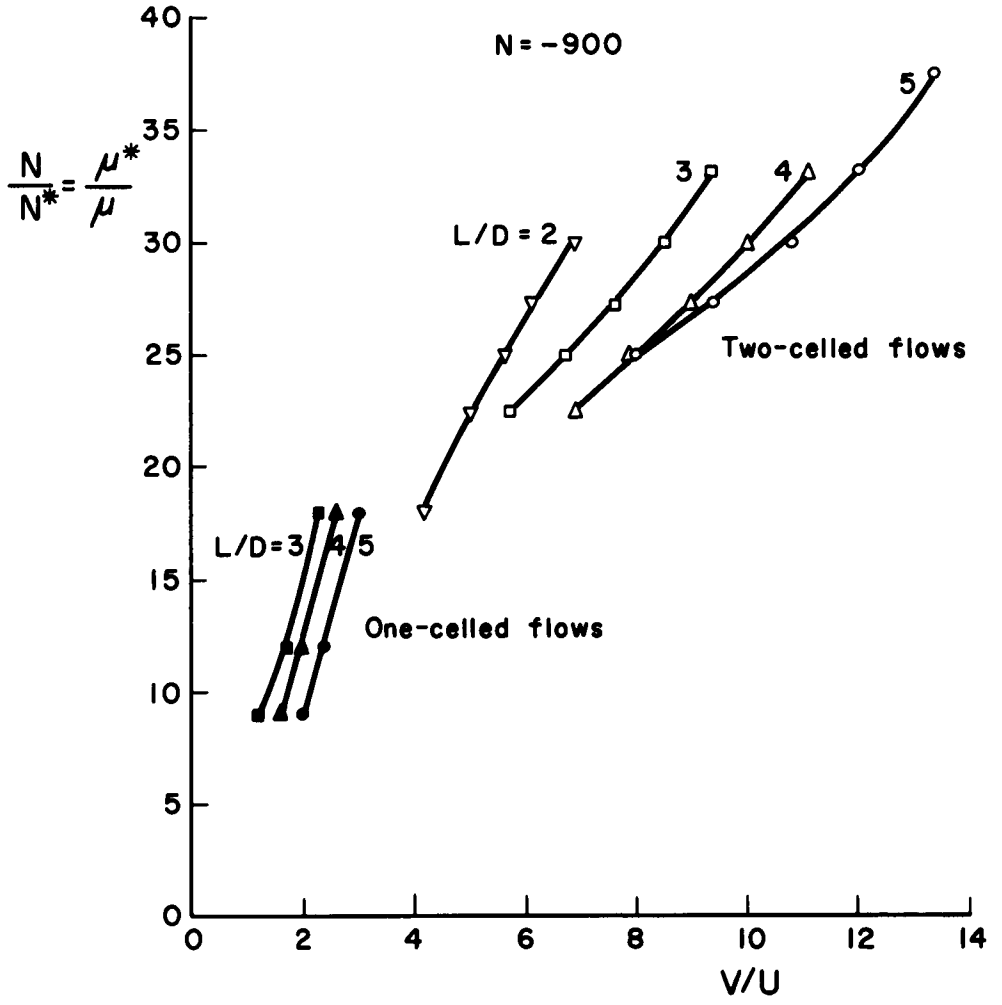

Figure 24. Ratio of effective to molecular viscosity as a function of V/U.

indicates an increase in effective viscosity which is roughly proportional to V/U.

One final point should be made before bringing this discussion of the experimental results to a close. This point has to do with the self-consistency and accuracy of the data. The general agreement between the measured static pressure drops and the pressure drops shown in figure 21 computed from the measured tangential velocity distributions can be taken as a measure of the accuracy of this velocity distribution data. Since, in general, very small changes in the tangential velocity near the center of a vortex cause large changes in the static pressure drop across the vortex it may be concluded, in view of the general agreement of the results, that the tangential velocity distributions measured near the center of the vortices in this study are, in all probability, reasonably accurate.

8. Conclusions

As a result of the experimental study of the flow in simple cylindrical vortex chambers completely open at one end that has been presented in the preceding sections, the following conclusions may be drawn:

(1) For turbulent vortices within cylindrical vortex chambers having length-to-diameter ratios in the range $0 < L/D < 5$, the primary parameter governing the character of the flow is V/U; that is, the ratio of a characteristic tangential to a characteristic radial velocity. This is in marked contrast to the behavior of laminar vortices where in addition to V/U the radial Reynolds number $N = UR/\nu$ is a most important parameter.

(2) For turbulent flow in vortex chambers in the above L/D range, the establishment of a two-celled vortex configuration is dependent on V/U alone. In particular, a second cell will begin to be established in any such vortex when the ratio of characteristic tangential to radial velocities exceeds approximately 3.

(3) It appears that turbulent vortices behave in an effectively more and more viscous manner the higher the ratio V/U becomes.

(4) The experimental results tend to give general support to the conjectures concerning the nature of three-dimensional turbulent vortices given in Sections 3 and 4 of the present paper.

REFERENCES

Donaldson, C. duP. 1956 Solutions of the Navier-Stokes equations for two- and three-dimensional vortices. Ph.D. thesis, Princeton University.

Donaldson, C. duP. 1961 The magnetohydrodynamic vortex power generator: Basic principles and practical problems. ARAP Rept. No. 30, Princeton.

Donaldson, C. duP., and Sullivan, R. D. 1960 Examination of the solutions of the Navier-Stokes equations for a class of three-dimensional vortices. Part I: Velocity distributions for steady motion. AFOSR TN 60-1227. Also Proceedings 1960 Heat Transfer and Fluid Mechanics Institute, Stanford.

Kendall, J. M., Jr. 1962 Experimental study of a compressible viscous vortex. JPL Tech. Rept. 32-290, Calif. Inst. of Technol.

Keyes, J. J., Jr. 1960 An experimental study of gas dynamics in high velocity vortex flow. Proceedings 1960 Heat Transfer and Fluid Mechanics Institute, Stanford.

Lamb, H. 1932 Hydrodynamics, 6th ed. New York: Dover Publications.

McCune, J. E., and Williamson, G. G. 1961 A preliminary study of the structure of turbulent vortices. ARAP Rept. No. 32, Princeton.

Ragsdale, R. G. 1960 NASA research on the hydrodynamics of the gaseous vortex reactor. NASA TN D-288.

Rosenzweig, M. L., Ross, D. H., and Lewellen, W. S. 1962 On secondary flow in jet-driven vortex tubes. J. Aerospace Sci., Vol. 29, No. 9.

Schowalter, W. R., and Johnstone, H. F. 1960 Characteristics of the mean flow patterns and structure of turbulence in spiral gas streams. AIChE J., Vol. 6, No. 4.